CRYSTALLOGRAPHIC AND SPECTROSCOPIC STUDIES ON THE COMPLEX OF CYTOCHROME C PEROXIDASE AND CYTOCHROME C

A Dissertation
Presented to the Faculty of the Graduate School
of Cornell University
in Partial Fulfillment of the Requirements for a Degree of
Doctor of Philosophy
by
Thomas Murray Payne
January 2014

Crystallographic and Spectroscopic Studies on the Complex of Cytochrome c Peroxidase and Cytochrome c

Thomas Payne, Ph.D.

Cornell University, 2014

Electron transfer (ET) is a ubiquitous process that underlies the physics of biology. Photosynthesis, respiration, and metabolism all require careful movement of electrons across long distances to generate the energy and chemical compounds necessary for life. Most electron transfer is controlled by proteins, which guide electrons to their destination through small jumps along a carefully arranged network of cofactors.

Cytochrome c Peroxidase(CcP) is a yeast protein that converts hydrogen peroxide to water, in a reaction catalyzed by reduction from Cytcochrome c (Cc). In the process of converting hydrogen peroxide to water, CcP generates a tryptophanyl radical on W191. This radical acts a "hopping site" for electron transfer, bridging the gap as a stepping stone between the hemes of Cc and CcP. In this study, we show that tyrosine (W191Y) can act as an effective hopping site in the same location, but that phenylalanine (W191F) cannot. Through transient absorption spectroscopy, we measure the rates of photoinitiated electron transfer from Zn-substituted CcP to Cc and back, and determine the rates of ET from Cc to W191F CcP, where the ET rates are such that the charged-separated intermediate can be observed. From these measurements, we calculate the reorganization energy of the reaction and determine that ET falls in the Marcus inverted region. We also observe the effect of ionic strength on complex formation and ET kinetics.

Through X-ray crystallography, we solved the structure of the various CcP mutants in complex with Cc, including the W191G mutation, which creates an empty cavity where other small compounds will bind. We showed that these compounds, although similar in structure to tryptophan and tyrosine, do not rescue peroxidase activity, and conclude that a hopping site must not only have the correct potential, but also be held stably in position and perhaps even covalently bonded to the electron acceptor.

BIOGRAPHICAL SKETCH

Thomas Murray Payne was born on November 11, 1983 to Charles Franklin Payne and Ruby Krabill Payne in Corpus Christi, TX. Growing up in Baytown, TX, he attended Sterling High School and discovered he enjoyed learning about physics and mathematics. Thomas attended college at the University of Texas at Austin, where he studied physics and computer programming, ultimately obtaining a BS in Physics in 2007. While studying at UT, Thomas performed research with Dr. Greg Sitz, working on an atomic-level Newtonian computer simulation of the interactions of methane with metal surfaces, eventually writing a thesis about it. Although originally he considered teaching high school physics, Thomas decided that he wanted to continue to learn science. Of all the areas of research Thomas had learned about, the applications of physics in the field of biology were the most fascinating, as they gave Thomas the opportunity to learn about an entirely new field.

Thomas was accepted into Cornell University at Ithaca's Biophysics Ph.D. program in 2007. He rotated in the labs of Brian Crane, Manfred Lindau, and Holger Sondermann. While each was a positive experience, he found the research project in Brian Crane's laboratory to be the most interesting, and Brian agreed to be his advisor. While in the Crane group, Thomas primarily worked on measuring electron transfer rates between cytochrome c peroxidase and cytochrome c using protein crystallography and transient absorption spectroscopy. He also worked on characterizing the ability of the protein azurin to bind iron, using x-ray absorption spectroscopy. Thomas completed his thesis in 2013 with great help from his labmates and advisor.

To my mother and father.

ACKNOWLEDGEMENTS

I would like to foremost thank Brian Crane, for accepting me into his group and being very, very patient with my progress over the years. I couldn't have asked for a better advisor. I'd like to thank Joanne Widom for training me in very basic lab techniques, and later for helping me troubleshoot the more complicated experiments. To Abiola and Sudhamsu, thank you for making me feel so welcome when I joined the lab and teaching me what you knew. The pleasure of working with you two was a substantial reason for my joining the lab.

I'd like to thank Xiaoxiao and Anand for being terrific, supportive lab mates and friends. I'd also like to thank Sarah Chobot Hokanson for her friendship and her skill. I learned quite a bit from observing her talent and professionalism. I'd like to thank my undergrad, Nancy Li, for being so unbelievably diligent. The amount of work that you put in on your difficult task is incredible. I'd like to thank Estella for all the work and quick learning she did to help me complete my thesis on time, and I wish her the best of luck on this project in the future. I'd like to thank my committee members, Lois Pollack and Peng Chen, for being supportive and accommodating and giving good advice over the years. And I'd like to thank my other lab mates: Ria, Ken, Craig, Greg, Karen, Alise, Camille, Mike, Peter, Dipanjan, Bee, and Anna.

I'd like to thank all the great friends I've made in Ithaca: Andrew, my friend and roommate, who helped me blow off steam at the end of the day; Alex, Molly, Megan, Nick, Amber, and Jeremy for all the fun times drinking; Joe, for being my confidant; Doug, for helping me through a real rough patch; and Phillip, for showing me how to have a good time. Lastly, I'd like to thank my parents, for always loving me and supporting me through everything that's happened in my life.

TABLE OF CONTENTS

LIST OF FIGURES

LIST OF SCHEMES

LIST OF TABLES

LIST OF ABBREVIATIONS

Cc – Cytochrome c

CcP – yeast Cytochrome c Peroxidase

DTT – dithiothreitol

ET – Electron Transfer

Fe(II) – Heme bound iron in the 2+ oxidation state; “reduced” iron

Fe(III) – Heme bound iron in the 3+ oxidation state; “oxidized” iron

Fe(IV) – Heme bound iron in the 4+ oxidation state double-bonded to oxygen; oxyferryl heme

FeCcP – CcP with heme as its cofactor

H175 – Coordinating histidine in CcP

I – ionic strength

KPi – Potassium phosphate buffer

NaPi – Sodium phosphate buffer

PCET – proton-coupled electron transfer

W191 – Tryptophan 191 in CcP

$W191^{+}$ - W191 in a cationic radical state

ZnCcP – CcP with ZnPor as its cofactor

ZnCcP* - ZnCcP in the excited triplet state

ZnPor – Zinc-protoporphyrin IX

$ZnPor^{+}$ - ZnPor in a cationic radical state

Chapter 1

Measurement of the Marcus Inverted Region in the Electron Transfer Kinetics of Zinc-Substituted Cytochrome c Peroxidase and Cytochrome c

1.1 Introduction

Electron transfer (ET) is a physical process that underlies the chemistry of life. The making and breaking of covalent bonds requires the local rearrangements of electrons in molecular orbitals as they band together to stabilize nuclei in localized or delocalized configurations. Over short distances, electrons rapidly rearrange to minimize coulombic energy. Occasionally, as lightning demonstrates, electrons can move great distances over vast insulating voids if the potential differences are high enough. But for molecular systems electrons generally stay localized, until outside forces intervene.

Much of the machinery of life exists for the purpose of relocating electrons for the good of the cell. Most of the time the processes begin by startling an electron out of its comfortable resting place and corralling it along a downward potential slope. The electron transport chain of photosynthesis, for example, begins when a photon forcibly ejects an electron from chlorophyll (Burda, 2007). The electron finds itself leaping from cofactor to cofactor, which are all carefully arranged and tuned by their protein environment to be more stabilizing than the last, until the electron reduces a diffusible organic moiety (plastoquinone) that can stably shuttle it along the membrane to the next photosystem. During this process, electrons will help generate a molecule of ATP and

two of NADPH, which will power the progression of countless more electrons around the cell to generate the dynamics of life.

Of interest to us is how the proteins manage the impressive task of guiding these charged particles to a specific destination and purpose. The focus of our study is two proteins from yeast: cytochrome c peroxidase (CcP) and cytochrome c (Cc), which have long served as a tractable model system to study the parameters that underlie protein electron transfer. CcP spends two electrons to convert a poison (peroxide) generated by the processes of aerobic respiration to harmless water, and multiple copies of Cc deliver electrons to catalyze this reaction(M. A. Miller, 1996). In the grand tradition of scientists of condensing a complicated problem down into more simple elements, studying the electron transfer from Cc to CcP will help illuminate key aspects all biological ET reactions.

Cytochrome c Peroxidase Mechanism

CcP is found in the intermembrane space of yeast mitochondria(A. N. Volkov, Bashir, Worrall, & Ubbink, 2009). Recombinantly expressed in *E. coli* without its N-terminal transit peptide, it is a 296 amino acid protein with a molecular weight of 34.5 kDa. Its primary activity is to convert hydrogen peroxide to water. CcP is stable as an apoprotein but usually contains one heme molecule, coordinated to the protein with

H175, which acts as an axial ligand to the iron(Pelletier & Kraut, 1992). The mechanism of action is described in Scheme 1:

$$Fe(III)CcP + HOOH \rightarrow Fe(IV=O),W191^{+}CcP + H_2O$$

$$Fe(IV=O),W191^{+}CcP + Fe(II)Cc \rightarrow Fe(III),W191^{+}CcP + Fe(III)\ Cc$$

$$Fe(III),W191^{+}CcP + Fe(II)Cc \rightarrow Fe(III)CcP + Fe(III)\ Cc$$

Scheme 1.1: Peroxidase Activity of CcP and Cc

The Fe(III) oxidation state of the heme binds hydrogen peroxide, which reacts to form an oxyferryl species on the heme and releases one of the peroxide oxygen atoms as a water molecule. During this process, tryptophan 191 (W191) is oxidized and forms a long-lived, stable radical(M. A. Miller, 1996). This $Fe(IV=O),W191^{+}$ CcP state is referred to as Compound 1 (Cpd1). Cpd1 is reduced by two separate copies of Fe(II) Cc and is returned to the resting state, ready to bind hydrogen peroxide once more.

Although there was initially much debate over the interaction between CcP and Cc, the crystal structure by Pelletier and Kraut(Pelletier & Kraut, 1992) of the CcP/Cc complex first identified the binding domain. The two proteins are brought together by hydrophobic interactions and stabilized by charged amino acids on the surface of the proteins. Charge-reversal mutations on this binding interface have been shown to significantly decrease Cc binding to CcP(Pearl, Jacobson, Arisa, Vitello, & Erman, 2007), and NMR measurements find that Cc spends 70% of the time spent in complex

with CcP at the same binding interface(Alexander N Volkov, Worrall, Holtzmann, & Ubbink, 2006), supporting the conclusion that the interaction in solution mirrors that seen in the crystals.

Marcus theory provides a framework to model electron transfer reactions in a semi-classical manner, and for high temperature, non-adiabatic processes the rate constant for ET is given by(Marcus & Sutin, 1985):

$$k_{ET} = \frac{2\,\pi}{\hbar}\frac{1}{\sqrt{4\pi\lambda k_B T}}\langle H_{DA}^2\rangle e^{-\frac{(\Delta G+\lambda)^2}{4\lambda k_B T}}$$

where k_B is the Boltzmann constant, T is the temperature, $\langle H_{DA}^2\rangle$ is the electronic coupling, λ is the reorganization energy, and ΔG is the driving force. $\langle H_{DA}^2\rangle \propto e^{-r}$, where r is the distance between the donor and the acceptor molecules. The greater the distance, the lower the rates of electron transfer. Typical distances for donor-acceptor separation in biological electron transfer fall within 14 Å (Page, Moser, Chen, & Dutton, 1999). The reorganization energy λ is formally the cost in free energy necessary to distort the nuclear configurations of the reactants to those of the products without transferring charge and reflects the energetics associated with restructuring the system upon electron transfer. The Marcus treatment models the forces that contribute to reorganization as having harmonic potential surfaces. For example, a histidine ligand will bind itself closer to a Fe(III) than it will to a Fe(IV=O) atom. The driving force, $-\Delta G$ is the free energy change associated with the net reaction. It is often expressed as the difference in redox potentials between the donor and acceptor. Downhill potential powers the electron transport chain and other biological ET reactions.

One important result of Marcus theory is that the rate is maximum when $-\Delta G = \lambda$, and that when $-\Delta G > \lambda$, ET will actually become slower. This effect arises because the activation free energy for ET becomes minimal when the potential surface for the product configuration intersects the equilibrium position on the reactant configuration surface. Although it seems counterintuitive that ET would become slower at a stronger driving force, this so-called "inverted effect" has been proven unequivocally for small molecule electron transfer reactions, when the donor and acceptor sites are held at rigid separation(J. Miller, Calcaterra, & Closs, 1984).

The role the reorganization energy plays in biological ET reactions has not been widely investigated, not least because it is difficult to measure. The distance *r* and driving force ΔG are directly observable, but λ and the coupling constant $\langle H_{DA} \rangle$ can only be calculated once all the other parameters are known. The reorganization energy is potentially as important as the driving force in the progress of biological ET reactions. In Photosystem 1, for example, at two early steps the protein moves downstream between cofactors with unfavorable driving forces(Burda, 2007). It may be that the proteins have tuned reorganization energies of the cofactors so that ET occurs at appreciable rates despite relatively low driving forces. In order to fully understand inter-protein ET, we must understand how the protein environment tunes the reorganization energy of these cofactors.

In biological systems, the existence of the inverted region remains in dispute. Work on intramolecular ET in proteins such as Cc and azurin by Gray et. Al. show that above a certain driving force, ET rates plateau instead of decreasing as predicted(Bjerrum et al., 1995). However, the inverted region was detected in collisional ET of small, artificial copper-binding proteins that were photoexcited by ruthenium-tags(Hong et al., 2006). Measurement of the inverted region in interprotein ET in a biologically relevant system would help establish the specificity of redox potential tuning necessary for efficient biological reactions.

Cc and CcP have long been used as models for studying electron transfer in proteins. In one set of studies, photoexcitable ruthenium tags have been attached to various places on Cc and the rates of ET between the tags and the heme of Cc measured to deduce the effect of the protein environment on k_{ET} (Bjerrum et al., 1995). In another study, ruthenium-tagged Cc was used to reduce Cc and observe the reduction of CcP Cpd1(Wang et al., 1996). Approaching the system from another direction, Hoffman et. Al. devised a system where the heme of CcP has been replaced by zinc porphyrin (ZnPor) and the rates of ET between the excited triplet state of ZnPor and Fe(III) Cc have been measured, both in solution and crystals of the complex (Ho, Sutoris, Liang, Margoliash, & Hoffman, 1985; Seong A Kang, Marjavaara, & Crane, 2004). From these studies we know that ET between the Cc and CcP heme is facilitated by the W191 radical. The crystal complex has the edge of the Cc heme facing the surface of CcP,

with the two porphyrins at an edge-to-edge distance of about ~16 Å. W191 is slightly closer to the Cc heme, at a distance of ~14 Å, within the distance for efficient ET(Pelletier & Kraut, 1992). The W191 radical provides a potent driving force at closer distance, and it has been shown that mutation of W191 to phenylalanine or glycine greatly reduces both rates of ET and peroxidase activity (Hays Putnam, Lee, & Goodin, 2009; Seifert, Pfister, Nocek, Lu, & Hoffman, 2005).

Molecular dynamics calculations by David Beratan's group indicates that past rates of charge recombination between Cc and ZnCcP can be explained if the kinetics are occurring in the Marcus inverted region(Beratan, 2013). In this work, we present further evidence of inverted ET in this system and measurements of the electronic coupling and reorganization energy.

1.2 Methods

Mutagenesis

Cytochrome c Peroxidase (CcP) was cloned into the ppSUMO vector, a pet28 derivative vector obtained with thanks from Dr. Holger Sondermann (Dept. of Molecular Medicine, Cornell University). The ppSUMO vector introduces a His-tagged version of the SUMO protein to the N-terminus of CcP to aid in recombinant expression. SUMO is a small protein that when fused to a target increases protein expression levels and solubility (Panavas, Sanders, & Butt, 2009). The SUMO tag is removable by cleavage with the protease ULP-1. The restriction sites BamHI and XhoI were used to insert the gene into

the ppSUMO multiple cloning site. Because the WT sequence of the gene for CcP contained a BamHI restriction site, a silent mutation was introduced as shown in Figure 1.1.

Figure 1.1: Silent mutation in the CcP gene. To clone CcP into the ppSUMO vector, a BAMHI site had to be removed by adding a silent mutation. Shown at top is the location on the gene of the mutation, and the primer used on bottom.

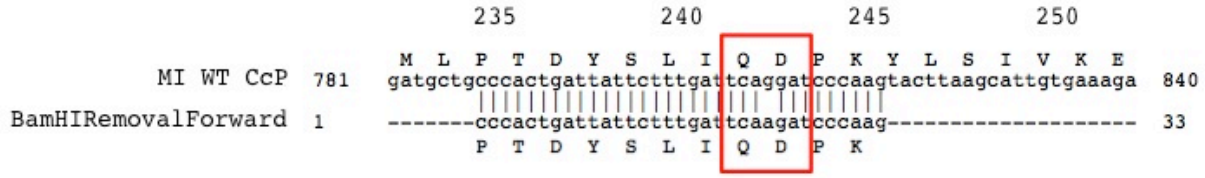

The following primers were used to remove the native BamHI site via PCR, and then to introduce BamHI and XhoI sites to the 5' and 3' ends of the CcP gene, respectively. The primers are displayed 5' to 3' and the introduced nucleotides are in lowercase.

BamHI Removal Coding – CCCACTGATTATTCTTTGATTCAaGATCCCAAG

BamHI Removal Anticoding - GCTTAAGTACTTGGGATCtTGAATCAAAGAATAATCAG

BamHI Addition Coding – gagcacggatccATGATCACCACGCCGCTCGTTCATGTCGCCTCTGTCG

XhoI Addition Anticoding – acacacctcgagTTACTCACAGGCTTTTTTCAAGTAGG

Once the CcP gene was cloned into the ppSUMO vector, mutations were made using the QuikChange protocol (Stratagene) with the following primers, printed 5' to 3'. The altered nucleotides appear in lowercase.

W191G Coding – CGAAGGGCCAgGGGGAGCCGCTAACAACGTC

W191G Anticoding – GGCTCCCCcTGGCCCTTCGTATCCAGAGTTC

W191F Coding – CGAAGGGCCATttGGAGCCGCTAACAACGTC

W191F Anticoding – GGCTCCaaATGGCCCTTCGTATCCAGAGTTC

W191Y Coding – CGAAGGGCCATacGGAGCCGCTAACAACGTC

W191Y Anticoding – GGCTCCgtATGGCCCTTCGTATCCAGAGTTC

Mutants of yeast iso-1 cytochrome c were constructed using the QuikChange protocol using the gene in the vector PBTR1 as the template. PBTR1 is a bacterial expression vector that includes the CYC1 gene for yeast iso-1-cytochrome c with mutation C102S (hereby referred to as WT) and CYC3, a heme lyase that helps form the thioether bonds that connect the heme to the polypeptide via two native Cys residues (Pollock, Rosell, Twitchett, Dumont, & Mauk, 1998). The following primers were used to create the site-directed mutants:

yCc Y48K Coding – GCTGAAGGGTATTCGaAaACAG

yCc Y48K Anticoding – GATATTGGCATCTGTtTtCGAATAC

yCc Y48H Coding – GAAGGGTATTCGcACACAG

yCc Y48H Anticoding – GGCATCTGTGTgCGAATACC

yCc N52I Coding – CGTACACAGATGCCAtTATCAAG

yCc N52I Anticoding – CACGTTTTTCTTGATAaTGGCATC

Protein Purification

Cc was purified by the protocol described by Pollock et al (Pollock et al., 1998). The vector PBTR-1 was transformed into *E. coli* BL21 (DE3) cells and grown at 37º C in

lysogeny broth (LB) with 125 µg/mL ampicillin and 50 µg/mL δ-aminoleveulenic acid to accelerate heme production. The PBTR1 vector (Pollock et al., 1998) uses the *trc* promoter which is constitutively active and does not require induction. Cells were grown overnight at 37º C, harvested by centrifugation at 8000 RPM, and pellets were resuspended in 50 mM sodium phosphate, pH 8.0. The resuspended pellets were either frozen for storage or lysed by sonication. Lysate was spun at 22,000 RPM for one hour to remove insoluble cell detritus and the supernatant was loaded directly onto a HiPrep CMFF cation-exchange column, using an Äkta FPLC. The column was equilibrated and washed with 50 mM sodium phosphate, and then Cc was eluted from the column by a five column volume gradient of a buffer containing 50 mM sodium phosphate and 500 mM NaCl. All red-colored fractions were collected and concentrated using Millipore Amicon Ultra centrifugal concentrators (10 kDa cutoff) and then loaded onto a Superdex 75 size-exclusion column with 50 mM sodium phosphate and 500 mM NaCl as the running buffer. Red-colored fractions were concentrated, flash frozen, and stored at -80 C.

CcP was transformed into BL21 (DE3) cells and grown at 37º C in LB with 50 µg/mL kanamycin. When cells reached an OD of 0.8 – 1.2, they were induced with 100 mM IPTG, the temperature was reduced to 24º C, and cells were allowed to grow overnight. Cells were harvested by centrifugation at 8,000 RPM and the pellets were resuspended in 50 mM HEPES, 250 mM NaCl and 5 mM imidazole. Cells were lysed by

centrifugation and insoluble cell detritus was separated out by centrifugation at 22,000 RPM for one hour.

CcP was purified with a Ni-NTA column following the manufacturer's protocol (Qiagen). To cleave the SUMO tag, ULP-1 was added to the elution and allowed to incubate at 4º C overnight. The eluent was then dialyzed into lysis buffer and flowed over the Ni-NTA resin to allow the cleaved tag to bind and separate from the protein. The eluent was dialyzed back into HEPES buffer and run over the NiNTA column again to remove cleaved tag. CcP was then dialyzed in 100 mM potassium phosphate, pH 6.0, and loaded onto a HiPrep Q anion-exchange column on the FPLC. A 10 column-volume gradient of 100 mM potassium phosphate against 500 mM potassium phosphate (KPi) was used to separate the heme-containing CcP (FeCcP) from the apo-CcP. The apo-CcP elutes first and is collected for zinc-porphyrin incorporation. The FeCcP elutes second and is concentrated and stored at -80 C for enzymatic assays.

For zinc-protoporphyrin IX (ZnPor) incorporation, first the apo-CcP concentration was determined using the absorbance at 280 nm and the molar absorptivity coefficient ε_{280} = 55 mM^{-1} cm^{-1}(Yonetani, 1967). Then a fivefold excess of ZnPor was measured out and mixed in 10 mL THF with an equimolar amount of carbonyl-diimidazole for 2 hours. The THF was removed by rotovap and the activated ZnPor resuspended in 500 uL of DMF. This ZnPor solution was added to the apo-CcP and allowed to stir in the dark for 5 days at 4º C.

After five days, the solution was centrifuged to remove protein and unbound ZnPor which has precipitated, and the supernatant concentrated to < 10 mL. The protein sample was loaded onto the Superdex 75 size-exclusion column in 100 mM KPi to increase purity and to remove non-specifically bound ZnPor. The colored fraction was concentrated and loaded onto the HiPrep Q to separate the apo-protein from the zinc-porphyrin incorporated protein (ZnCcP) using the protocol described above to separate apo-CcP from FeCcP. Spectra of colored fractions were measured, with zinc incorporation evaluated by comparing the absorbance of the protein peak at 280 nm and the ZnCcP Soret peak at 432 nm (ε_{432} = 180 mM^{-1} cm^{-1})(Nocek et al., 1991). Fractions with a ratio of $A_{432}/A_{280} > 2$ were concentrated, flash frozen, and stored at -80º C for crystallization and spectroscopy.

Transient Absorption Spectroscopy

Oxygen will quench the ZnCcP excited triplet state and thus, care was taken to degas all samples and solutions and preparation of spectroscopic samples was carried out under anaerobic conditions. ZnCcP was mixed with 100 mM KPi, pH 7.0 to a concentration of 100 – 200 uM.

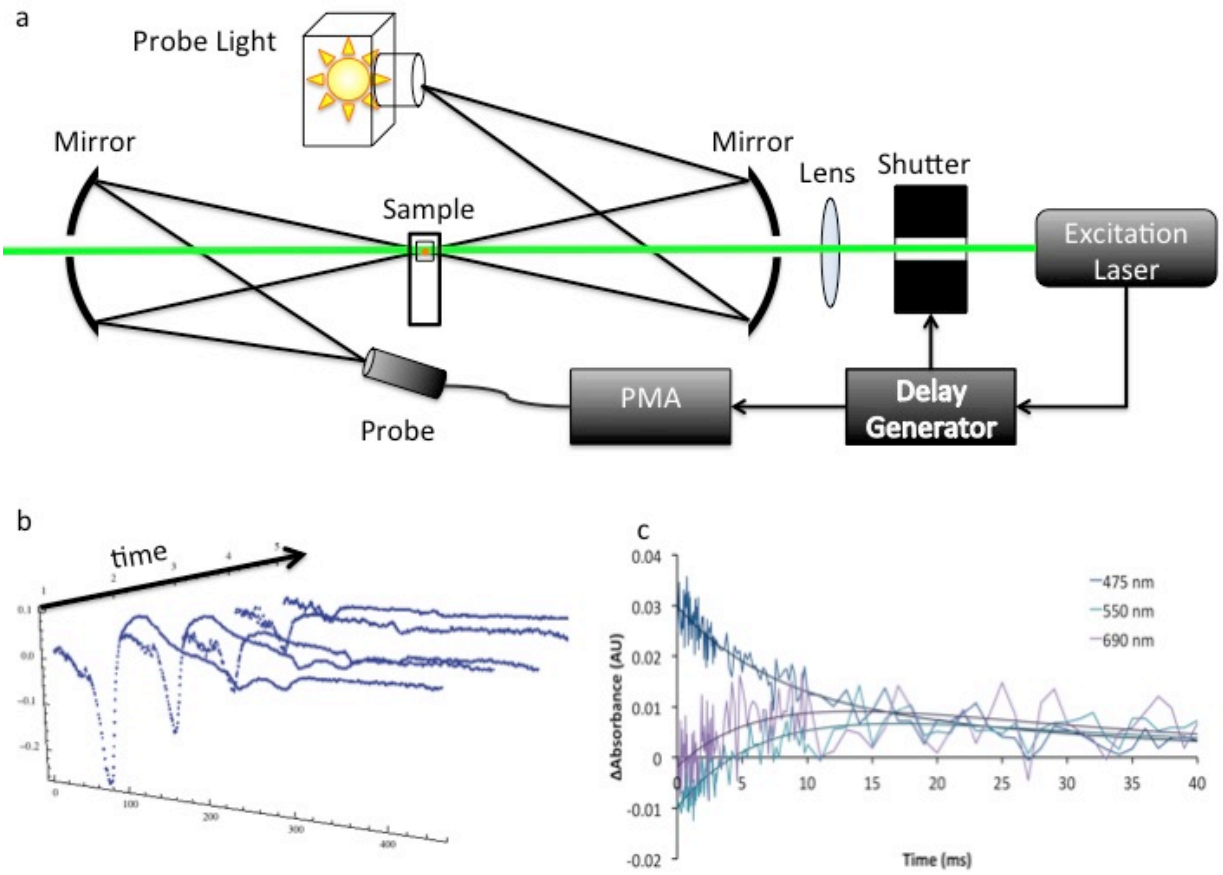

Figure 1.2: Spectroscopy Scheme. a) Diagram of the spectroscopy setup. White light from a Xe-arc lamp is directed through the sample and into the probe of the Photonic Multichannel Analyzer (PMA). A pulsed laser excites the sample and acts as a trigger for data collection. b) Full spectra (200 – 800 nm) are collected at various time points. Multiple measurements are averaged to achieve a high signal/noise ratio. c) Global analysis software is used to fit the data at multiple wavelengths simultaneously.

4 uL drops were placed on siliconized glass coverslips (Hampton) and were glued to glass slides using a ring of epoxy to form a gas-tight seal. Pathlength varied somewhat from sample to sample, but has been calculated to be about 0.5 mm on average.

Figure 1.3: Absorbance and fluorescence spectra of ZnCcP. Excited ZnCcP releases fluorescence at 600 nm and 640 nm (inset). Fluorescent efficiency at various excitation wavelengths was measured by tracking the light emitted at 600 nm. For spectroscopic study, samples are preferentially excited at the alpha band at 560 nm, although there is also sufficient excitation at 532 nm.

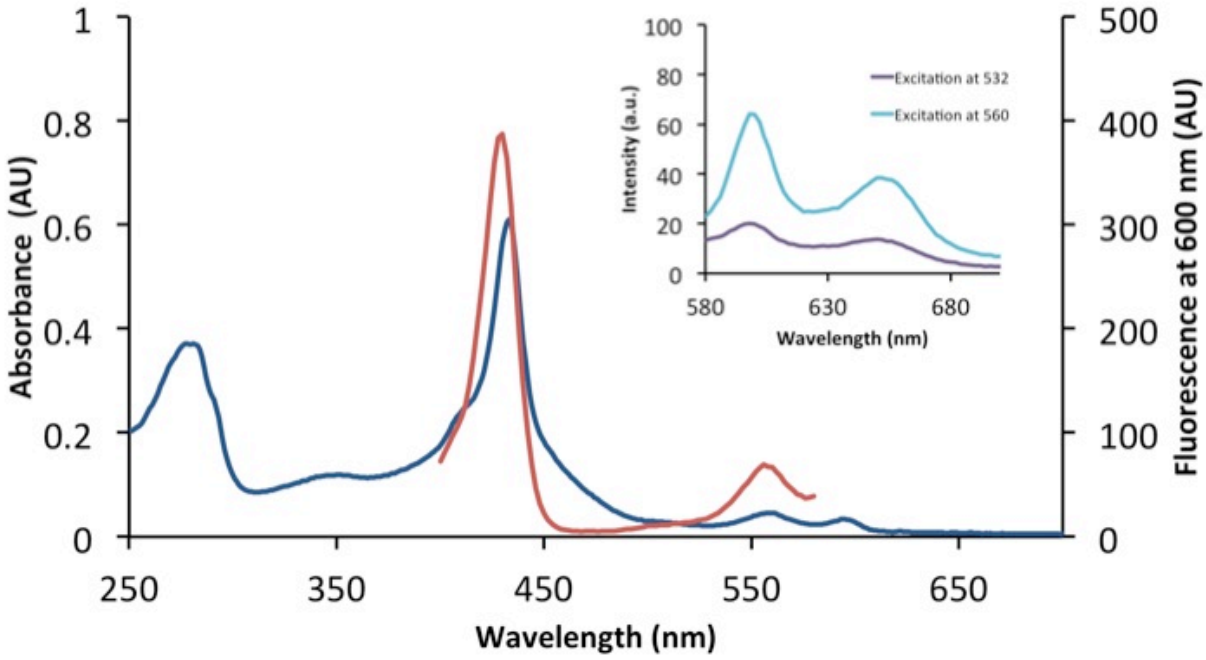

The spectroscopy apparatus is diagrammed in Figure 1.2. Samples were placed in the path of a probe light, provided by a 75-W Xe-arc lamp. Excitation light was provided either by a Opotek Opolette Nd:YAG laser tuned to 560 nm with approximately 2 mJ of power per 8 ns pulse, or a Continuum Surelight Nd:YAG laser providing light at 532 nm at approximately 5 mJ of power per 4 ns pulse. Both energies result in excitation of the zinc porphyrin, although 560 nm is more efficient due to the increased cross-section provided by the alpha-bands (Figure 1.3). Both lasers fire at 20 Hz. Exposure of excitation light in controlled by a Hamamatsu A6538 Optical Laser shutter, and the absorbance of the probe light is measured with a Hamamatsu Photonic Multichannel Analyzer (PMA). Unless otherwise specified, spectra collected by the PMA are from a

1-50 μs exposure time and are averaged 20 – 200 times, depending on the strength of the signal. The laser firing acts as the master trigger, with a Digital Delay Generator DG355 (Stanford Research Systems) controlling timing between the other elements.

To determine t_0, a 1 μs exposure time was used and spectra were taken every microsecond after the laser trigger until the scattered laser light was detected. The next μs in time was denoted t_0. Subsequent time points were then sampled randomly with an entire UV/Vis spectrum collected at each one. The time points are acquired in a random order to negate the effects of a photobleaching that may occur during data collection. To record a given time point, first N reference spectra are collected at the specified delay time (relative to t_0) where N is the number of spectra being averaged. Next, the laser shutter opens and N excited spectra are collected at the same delay. The software calculates the difference spectra as $\Delta A = -\log\left(\frac{Excited}{Reference}\right)$ and saves the result.

Scheme 1.2: ET Kinetics of ZnCcP for W191 and Y191. The zinc-porphyrin (ZnPor) bound to CcP is raised to the excited triplet state ($ZnPor^3$) by a 8 ns pulse of 532 – 560 nm light. $ZnPor^3$ CcP will then either decay back to the ground state at rate k_{zn}, or tunnel an electron to bound Fe(III) Cc, reducing it to Fe(II) Cc and leaving the ZnPor in a cationic radical state ($ZnPor^+$). The radical $ZnPor^+$ will rapidly oxidize nearby sidechain 191, and then charge recombination will occur through back ET from the Fe(II) Cc to the ZnPor($X191^+$), returning the system to the ground state. As $k_{eb} >> k_e$, the charge separated state depletes too quickly to observe.

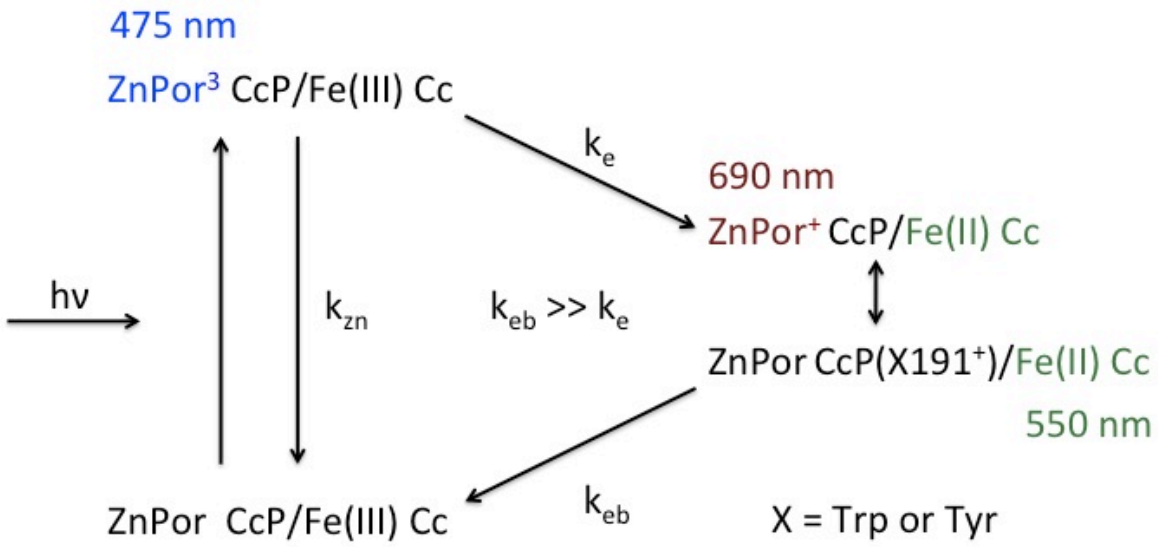

To process the data, data vectors across the wavelength range are reordered in time and subjected to global analysis by Glotaran(Snellenburg, Laptenok, Seger, Mullen, & van Stokkum, 2012). The data below 375 nm was discarded because little light at those wavelengths is transmitted through the optics to the PMA, and data above 750 was discarded for lack of spectral features. A baseline correction at the triplet state isobestic point 546 nm is applied(Seifert et al., 2005). Single-valued decomposition (SVD) of the multi-wavelength data was carried out to reconstruct the minimum number of spectroscopic (difference) states sufficient to describe the kinetic progress. In general, sequential reaction kinetics were assumed (see Discussion) and as such single, or double exponential terms were used to connect the spectroscopic states in time.

1.3 Results

To monitor the rates of electron transfer, we use a system first pioneered by Hoffman et. al. (Ho et al., 1985) and depicted in Scheme 2. The heme in CcP has been replaced with zinc protoporphyin IX (ZnPor), which can be excited to a long-lived triplet state by excitation at 532-560 nm light. Excited ZnPor substituted CcP (ZnCcP) will decay slowly back to the ground state with rate $k_{zn} \sim 100\ s^{-1}$. When oxidized Cc (Fe(III)Cc) is bound to ZnCcP, the excited ZnCcP (ZnCcP*) will be quenched via heme-to-heme electron tunneling to Cc with rate constant k_e. This produces a ZnPor cation radical ($ZnPor^+$) and reduced Fe(II) Cc. In wild-type CcP, $ZnPor^+$ will oxidize nearby W191 and generate an indole cation radical ($W191^+$). It is likely that the radical equilibrates extremely rapidly between the ZnPor and W191 or may be considered delocalized between the two centers(S. A. Kang & Crane, 2005; S. A. Kang, Hoke, & Crane, 2006; Seong A Kang et al., 2004). Analogous to biological peroxide reduction, the Fe(II)Cc can recombine with the ZnPor/$W191^{+\bullet}$ center in a back electron transfer (with rate constant k_{eb}) neutralizing the charge separation and returning the system to the ground state. In the wild-type system, k_{eb} greatly exceeds k_e, and as a result the charge-separated intermediate forms in vanishingly small amounts(S. A. Kang & Crane, 2005; S. A. Kang et al., 2006; Seong A Kang et al., 2004).

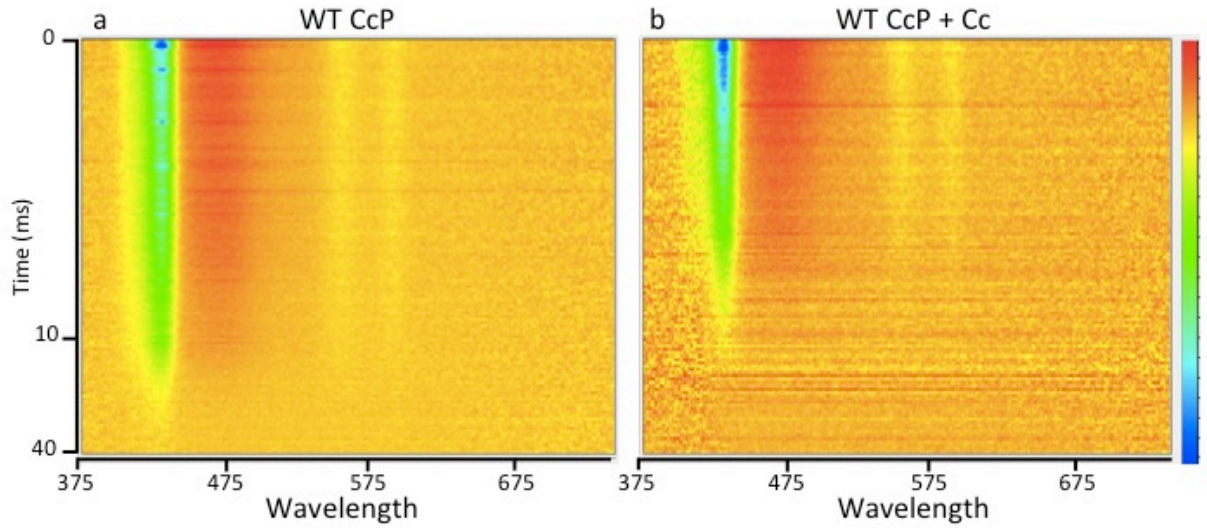

Figure 1.4: Time-dependent difference spectra of excited ZnCcP. a) Heat map of the difference spectrum of the excited state decay of ZnCcP. Blue to red coloring reflects negative to positive absorption, respectively. The difference spectrum is strongest at time t=0 ms, at the top of the chart, and decays over 40 ms to a flat line. Initial time points are space 50 µs apart, and the time interval increases over the course of the measurement. The exposure time to collect spectra is 50 µs. b) The excited state decay of WT CcP with Cc added. The excitation is measurably shorter lived.

For the first time, we report complete UV/Vis difference spectra of the participating species. A typical difference spectrum for the excited triplet state of wild-type ZnCcP is shown in the absence of Cc (Figures 1.4a and 1.5a). The difference spectra is characterized by a broad, positive peak at 475 nm and two negative alpha bands at 555 nm and 592 nm(Koloczek et al., 1987). A strong negative peak at 432 nm also appears, and to our knowledge has not been previously reported. The 432 nm, 555 nm, and 592 nm peaks correspond to absorption peaks in the visible spectrum of CcP (Figure 1.2), and their diminished intensity in the excited state reflects the change in the electronic state of ZnCcP. While the 432 peak is the strongest feature in the spectra, the 475 nm peak will be used to track the lifetime of the triplet state for several reasons. First, it is the wavelength used in previous studies(Ho et al., 1985; Seong A Kang et al., 2004),

and so is the best for comparison. Second, the appearance of the 432 nm difference peak can vary unpredictably. Figures 1.4a and 1.5a show its most common appearance, but the magnitude of the peak relative to the 475 peak is sometimes greater or much less, and it occasionally appears broader, narrower, or displays peak splitting. We currently do not understand the cause of this variation. The 475 nm peak, however, is very consistent in its shape and magnitude, and is unique to the triplet state and hence will be used for lifetime measurements.

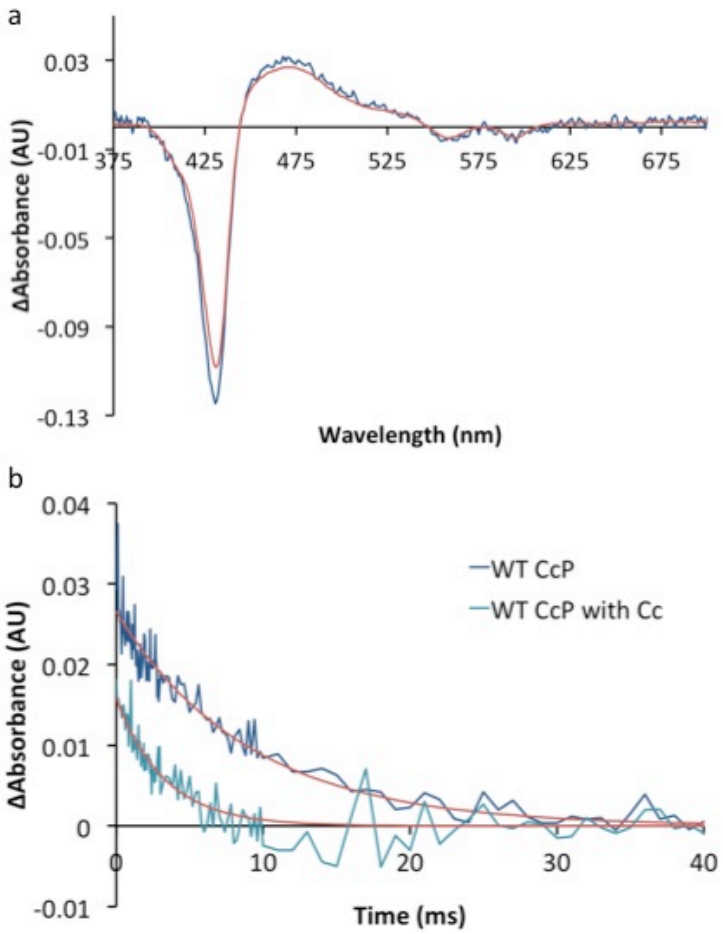

Figure 1.5: Profiles of the excited triplet state of Zn CcP. a) The difference spectrum of the excited state of ZnCcP at time t=0. Data is shown in blue , with the global fit shown in red. b) The absorbance at 475 over time for ZnCCP with and without Cc.

For a typical time course, data was collected from 0 to 40 ms with a 50 us exposure

time. The initial time points are taken every 50 us for the first four milliseconds, and then at increasingly broad time intervals after that. Figure 1.4 shows the UV/Vis range over a typical time course displayed as a heat map. Negative difference peaks are shown in blue and positive peaks in red. When ZnCcP is the only species in solution, the data fits well to a single exponential decay, and all spectral features decay at the same rate toward zero with an average rate of $k_{zn} = 114.49 \pm 4.13\ s^{-1}$.

Fe(III) Cc was added to solution in a two-fold excess to guarantee complex formation. As Figure 1.4b shows, the rate of triplet state decay increases in the presence of oxidized Cc, to a rate of $k_{obs} = 229.6 \pm 4.5\ s^{-1}$. Figure 1.5b compares the rates of the 475 nm peak decay in the presence and absence of Fe(III) Cc. To confirm that this increased triplet state quenching results from electron transfer to the Fe(III) Cc, the experiment was performed with Fe(II) Cc (Table 1). In the presence of Fe(II) Cc there was a small increase in decay rate, but not to the level of Fe(III) Cc. This is mostly likely due to a small fraction of reduced Cc in the oxidized Cc stock.

W191Y CcP shows behavior similar to wild-type CcP. The difference state spectrum is identical, and the rates are similar (Table 1). For both wild-type and W191Y ZnCcP, the spectra of the charge separated intermediate state could not be detected. Even for data sets taken with an exposure time of 1 μs, spanning from t = 0 μs to 400 μs, no intermediate state could be detected. This supports the conclusion that keb >> ke, and thus the intermediate will never build up to an observable extent.

Table 1.1: ET rates measured by transient absorption. CcP and Cc list the mutants measured. Unless otherwise stated, the Cc used was in the fully oxidized state. Cc E^0 is the redox potential measure vs. SHE. Ionization is the concentration of KPi pH 7.0 used in solution. Rates show the average and (standard deviation) of at least 3 samples for each rate. * $k_e = k_1 - k_{obs}$, where kobs is the rate of ZnCcP decay without Cc present.

				Single Exponential Fit	Double Exponential Fit		
CcP	Cc	Cc Potential	KPi (mM)	kobs	k1	k2/keb	ke*
WT			100	114.5 (4.1)			
WT	Reduced WT		100	148.9 (4.5)			
WT	Oxidixed WT	290	100	229.6 (12)			115.1 (13)
WT	Y48H	210	100	207.0 (51)			92.49 (51)
WT	N52I	232	100	259.0 (4.2)			144.5 (5.9)
WT	Y48K	407	100	160.9 (15)			46.36 (15)
W191G			100	113.1 (6.2)			
W191G	Reduced WT		100	97.4 (6.9)			
W191G	Oxidized WT	290	100	118.1 (9.5)	185.7 (9.9)	15.87 (1.5)	72.59 (12)
W191Y			100	112.1 (15)			
W191Y	Reduced Cc		100	153.7 (3.9)			
W191Y	Oxidixed WT	290	100	262.0 (15)			149.9 (21)
W191Y	Y48H	210	100	281.5 (3.9)			169.3 (15)
W191Y	N52I	232	100	281.7 (12)			169.6 (19)
W191Y	Y48K	407	100	193.3 (5.3)			81.14 (16)
W191F			100	102.4 (5.2)			
W191F	Reduced WT		100	132.9 (7.5)			
W191F	Oxidized WT	290	100		158.3 (7.8)	28.73 (4.5)	55.93 (9.3)
W191F	Y48H	210	100		223.6 (28)	23.69 (2.3)	121.3 (28)
W191F	N52I	232	100		250.4 (29)	24.44 (1.8)	148.0 (30)
W191F	Y48K	407	100		142.0 (9.3)	22.99 (4.1)	39 .58 (11)
W191F	Oxidized WT	290	30		287.5 (25)	49.05 (13)	185.1 (25)
W191F	Y48H	210	30		345.6 (24)	34.00 (4.5)	243.2 (24)
W191F	N52I	232	30		370.6 (7.8)	37.50 (4.7)	286.2 (9.4)
W191F	Y48K	407	30		289.2 (30)	45.77 (2.1)	186.8 (31)
W191F	Y48K	407	420		132.0 (4.9)	5.127 (1.3)	29.40 (7.1)
W191F	Y48H	210	420		119.6 (7.5)	5.638 (2.7)	17.27 (9.1)

It has been previously shown that W191F allows for detection of the intermediate state (Seifert et al., 2005), and our results confirm that. Alone, W191F produces an identical difference spectra to the wild-type, and decays uniformly at the same rate. However, in

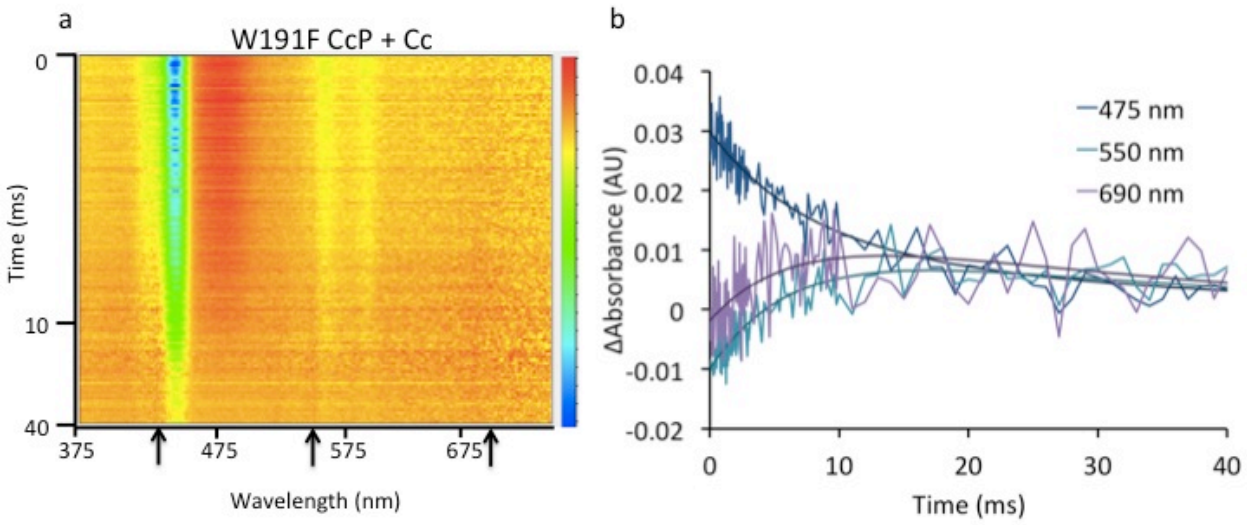

Figure 1.6: Detection of a charge-separated state. a) Heat map of the excited state difference spectra for W191F ZnCcP with Cc. Note the formation of darker bands at 416, 550, and 690 nm as time progresses. b) Time plots of the difference spectra at various wavelengths. 475 nm reflects the excited triplet state, 550 the reduced Cc, and 690 the porphyrin radical.

the presence of Fe(III) Cc, an additional spectral species is detected (Figure 1.6). At around 10 ms, positive peaks begin to appear at 416 nm, 550 nm, and a broad peak at 690 nm. These peaks appear as the triplet state disappears, and then they begin to decay back toward zero (Figure 1.6b). Using single value decomposition (SVD), the global analysis reveals two distinct Evolution Associated Difference Spectra, or EADS (Figure 1.7). The entire set of time dependent spectra observed in these measurements can be modeled as a superposition of these two EADS (van Stokkum, Larsen, & van Grondelle, 2004), dubbed EADS1 and EADS2. EADS1 is identical to the triplet state decay and is present at time t = 0 ms (Figure 1.7a). EADS2 appears as EADS1 disappears and is visible between 10 – 40 ms (Figure 1.7b). Fe(II) Cc is characterized by a Soret peak at 416 nm and alpha bands at 522 and 550 nm (Figure 1.7d). These match peaks those that appear in the second spectral species.

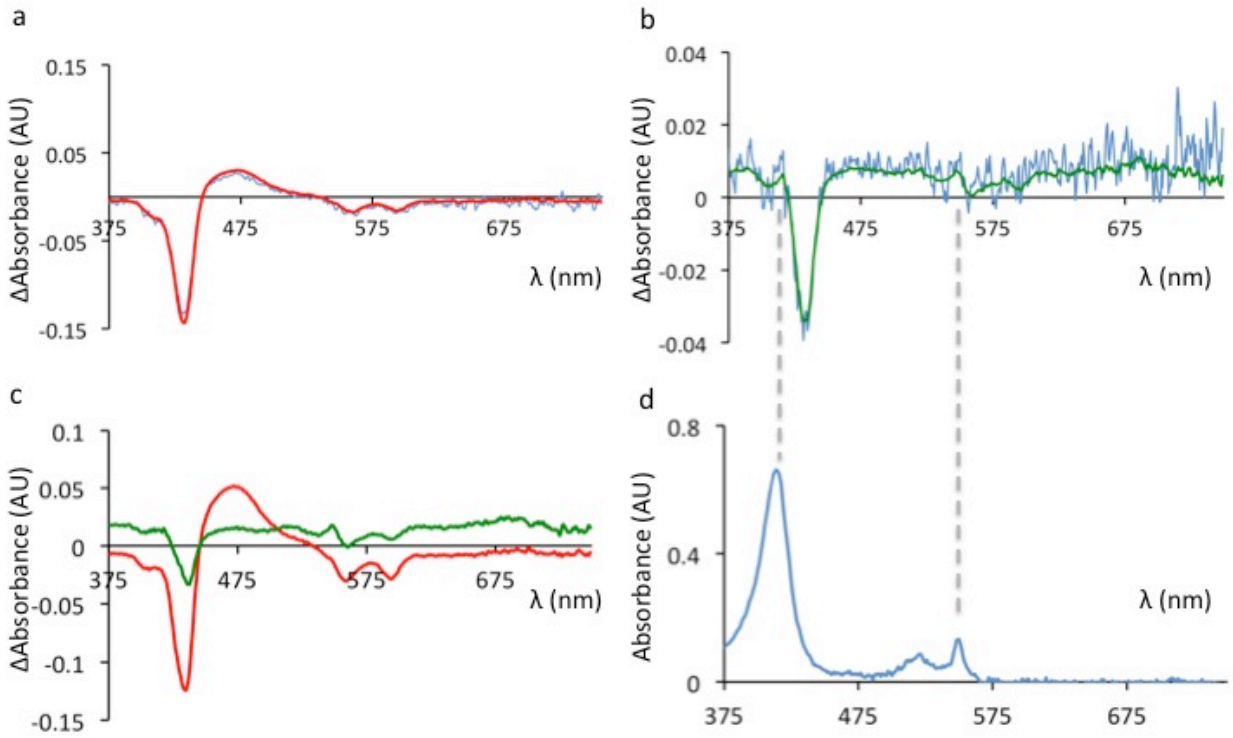

Figure 1.7: Evolution Associated Difference Spectra (EADS) of the charge-separated state a) Difference state spectra at time t = 0 of W191F ZnCcP with Fe(III) Cc. Recorded absorbances shown in blue, global fit shown in red. b) Difference state spectra at time t=18 ms. Recorded absorbances are in blue with the fit shown in green. New peaks at 416 and 550 nm are attributed to Fe(II) Cc, and the broad peak at 690 nm is characteristic of ZnPor+. c) EADS calculated by Single Valued Decomposition and global analysis. EADS1 is shown in red, EADS2 in green. d) The visible range absorbance spectra of Fe(II) Cc. Dotted lines shown where the Fe(II) Cc spectrum is visible in the time-resolved data.

The 690 nm peak is characteristic of a ZnPor radical [ref]. It can be inferred then that EADS2 reflects the formation of Fe(II) Cc and the ZnPor radical.

In tracking the appearance of Fe(II) Cc, the 550 nm peak was used because it is the strongest across all data sets. The 416 nm peak is noisier, because it is occluded by the 432 nm negative triplet state peak and because the probe light is weaker at that wavelength. EADS2 contains both the 550 nm peak and the 690 nm peak, and the global analysis models them as rising and falling at the same rate. This supports the

conclusion that forward ET occurs between ZnCcP and Fe(III) Cc, and that the charge recombines through back ET between Fe(II) Cc and $ZnPor^{+}$ CcP. To investigate the possibility that the ZnPor radical may form at a rate different than the Fe(II) Cc state, the data was modeled with three rate constants. However, the third EADS was always degenerate to the first two and produced no new species of unique spectral qualities or time evolution.

Forward and back ET rates calculated in this work are based on the rates of formation of EADS1 and EADS2. Because the 550 nm peak overlaps with the 555 nm negative peak, the absorbance at 550 nm alone cannot be used to track the formation of Fe(II) Cc. It may be possible to deconvolute the separate chemical species from EADS2 using target analysis(van Stokkum et al., 2004), but given the solid identification of the species involved, and our ability to extract the forward and reverse observed rate constants this is not necessary for our present purposes.

Because the sample preparation method causes a variable pathlength through the sample, it is difficult to precisely determine the concentration of the charge separated species. By following the formation of the 550 nm peak at the isobestic point 546 nm and using the molar extinction coefficient 28.2 mM^{-1} cm^{-1}(Chae Hee Kang, 1977), we estimate that between 1 – 3 % of the Fe(III) Cc present in the sample is reduced to Fe(II).

The rates of decay for states EADS1 and EADS2 are k1 and k2, respectively. The forward and back ET rates are calculated as

$$k_1 = k_{zn} + k_e \quad \textbf{(1)}$$

$$k_2 = k_{eb} \quad \textbf{(2)}$$

For interaction of W191F with WT Cc, k_e = 55.93 ± 9.3 s^{-1}, and k_{eb} = 28.73 ± 4.5 s^{-1}. Due to the slower speed of k_{eb} in this mutant, Scheme 2 is no longer valid. Scheme 3 describes the kinetics when $k_{eb} < k_{off}$.

For forward ET to occur, ZnCcP and Fe(III) Cc must be complexed together. At the ionic strength (I) present in this buffer (100 mM KPi ≈ 300 mM I), k_{off} approaches 10^4 s^{-1}. With keb measured at ~ 30 s^{-1}, Cc will leave the complex several hundred times before the charge recombines with ZnCcP. CcP shares equal affinity with Fe(II) Cc and Fe(III) Cc, and as Fe(III) Cc is in far greater abundance than Fe(II) Cc, after the forward ET $ZnPor^{+}CcP$ is likely to complex with Fe(III) Cc, and Fe(II) Cc is likely to complex with ZnCcP. Deconvoluting the ET rates from the on and off rates requires careful kinetic analysis (see Discussion section).

Scheme 1.3: ET Kinetics of ZnCcP for W191F. As in Scheme 2, ZnCcP is raised to an excited triplet state, and will either decay to the ground state or reduce bound Fe(III) CcP and develop a cationic radical on the ZnPor. However, with no sidechain available to oxidize, charge recombination must occur through tunneling from Fe(II) Cc heme to the ZnPor+, a much slower process. During this time, Fe(II) Cc can dissociate from the complex, and both proteins may bind with other molecules of Cc and ZnCcP with equal affinity. It is not until Fe(II)Cc and ZnPor+CcP bind together in the ET active complex that the reaction can end.

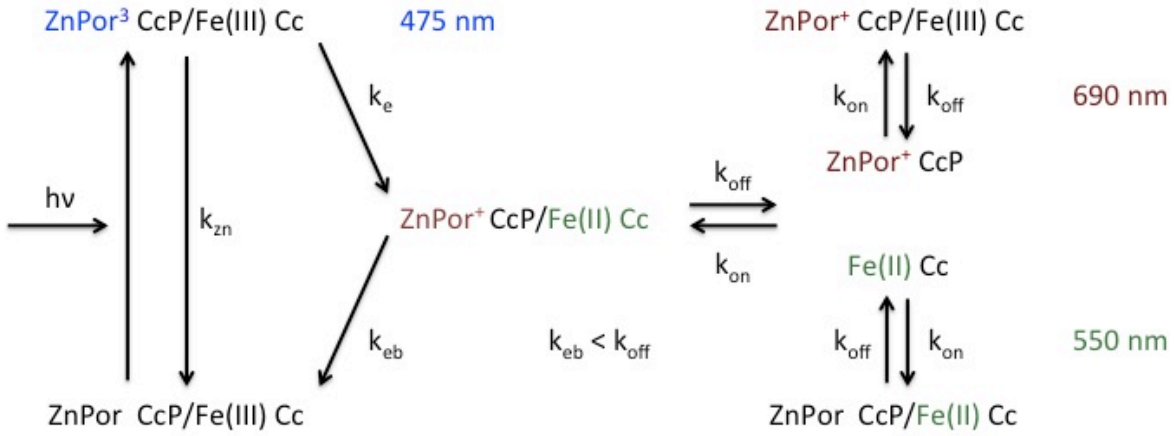

Driving force dependence of ET kinetics

To understand the effects of the driving force ΔG on ET, the kinetics of W191F CcP with several mutants of Cc were measured. The mutations are Y48H (E^0 = 210 mV), Y48K (E^0 = 407 mV), and N52I (E^0 = 230 mV). The potential of wild-type Cc is E^0 = 290 mV(Lett & Guillemette, 2002). Because Y48 and N52 are far from the binding interface of Cc with CcP, we do not believe the mutations will cause any steric hindrance to binding (Figure 1.8). It's also been shown that Cc binding to CcP is not affected by the Fe oxidation state, only by mutations to surface residues in the interface(Alexander N Volkov, Nicholls, & Worrall, 2011). This evidence indicates that these mutants of Cc

should bind to CcP with wild-type conformation and affinity. Indeed, the mutants are all highly active in the steady state peroxidase assay (Chapter 2).

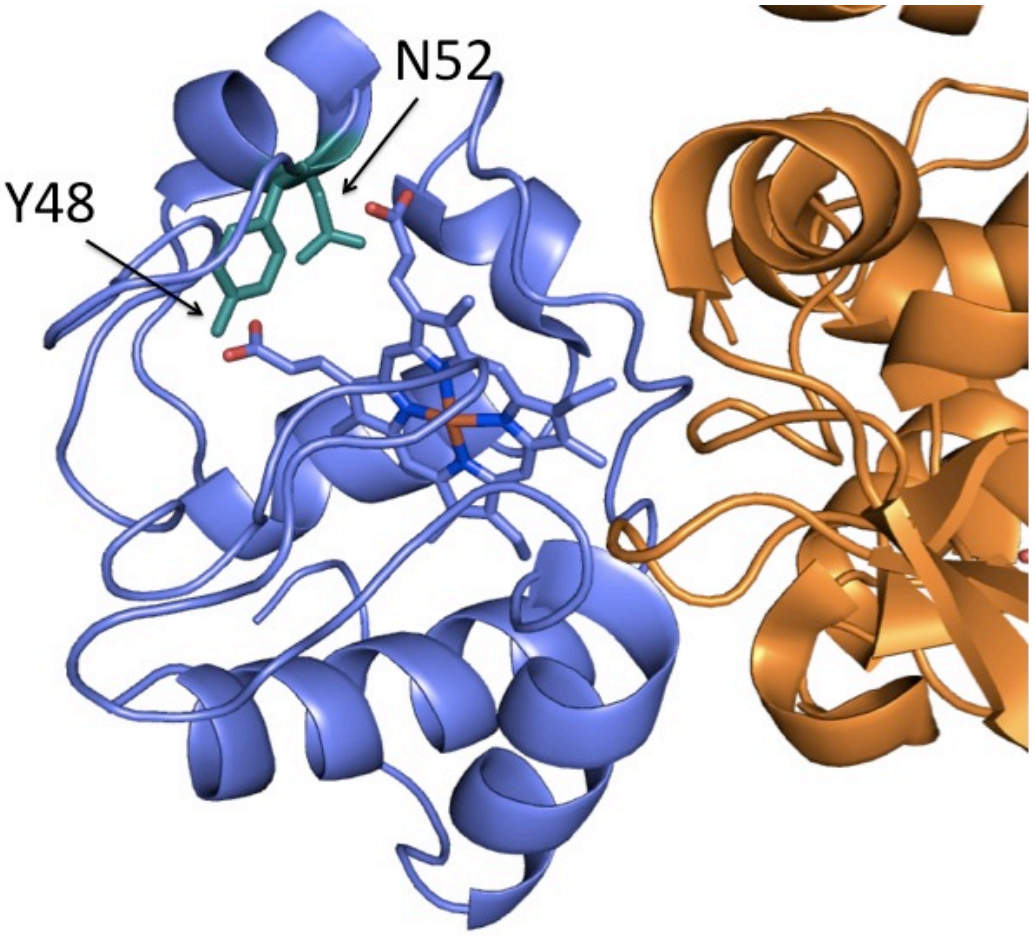

Figure 1.8: Cytochrome c Mutations. Residue substitutions at targeted residues Y48 and N52 of Cc (blue) alter the potential of the Cc heme without affecting the binding interface with CcP (orange).

All data sets with W191F CcP with a Cc mutant show EADS1 and EADS2 with the same spectral shape as with wild-type Cc. However, the values of k_1 and k_2 vary from mutant to mutant. The trends are discussed below where we argue that these differences

reflect alteration to the ET step itself. Table 1 shows the rates calculated, and Figure 1.9 shows the rise and fall of EADS1 and EADS2.

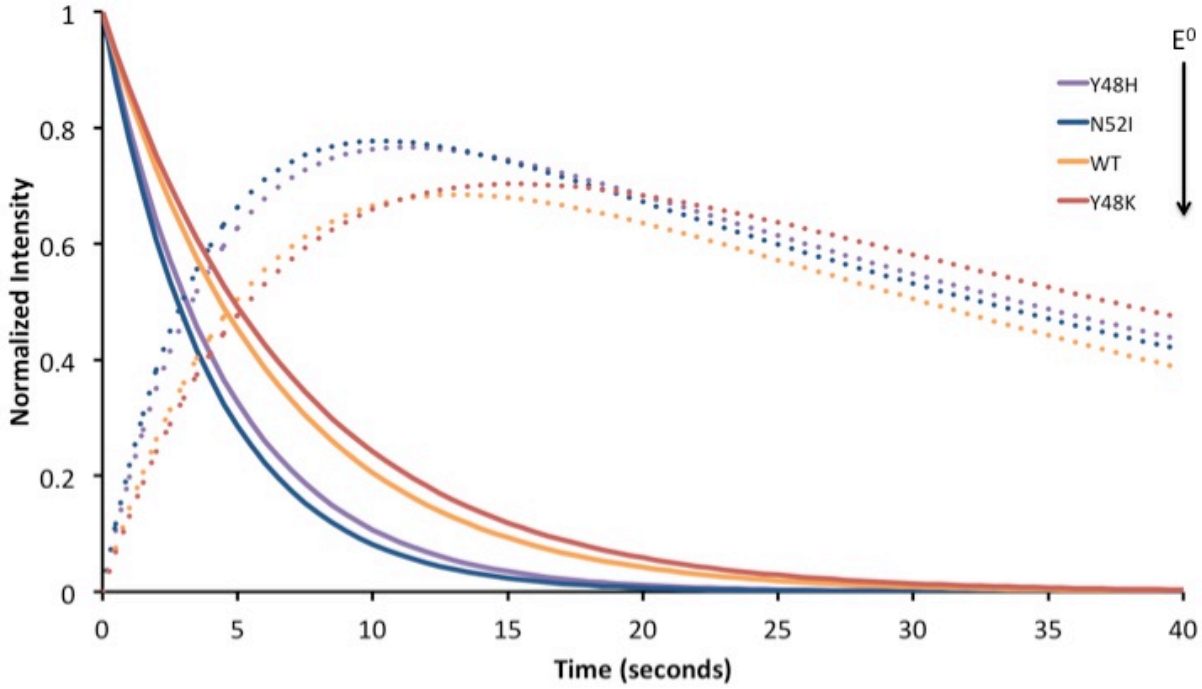

$$[A] = e^{-k_1 t}$$

$$[I] = \frac{k_1}{k_2 - k_1}\left(e^{-k_1 t} - e^{-k_2 t}\right)$$

Figure 1.9: Comparison of Cc mutant kinetics. Plots of the decay of the triplet state and formation and decay of the intermediate state. Cc mutants are listed in order of increasing potential. Curves were generated fitting the rate constants for each mutant with the equations shown. The triplet state decay [A] is represented by a solid line and the intermediate charge-separated state [I] by a dotted line.

W191G CcP alone behaves just like the wild-type, with a triplet state decay rate of 113.1 ± 6.2 s^{-1} that fits well to a single exponential decay (Figure 1.10). In the presence of

Fe(III) Cc, an intermediate state is detected, with EADS1 and EADS2 displaying similar spectra to W191F CcP. However, the rate of decay of EADS2 is altered with k_e = 72.59 ± 12 s^{-1}, and k_{et} = 15.87 ± 1.5 s^{-1}.

Figure 1.10: Excited state kinetics of W191G CcP. a) Heat map of the difference spectra of the excited state decay of W191G ZnCcP with Fe(III) Cc. Note the slow formation of bands at 550 and 690 nm. b) Time plots of the difference spectra at various wavelengths. 475 nm reflects the excited triplet state, 550 nm the reduced Cc, and 690 nm the porphyrin radical. c) Excited state difference spectra at time t=0. Recorded absorbances shown in blue, global fit shown in red. d) Excited state difference spectra at time t = 40 ms, where the peaks at 550 and 690 nm are easily observed. Global fit is shown in green. e) EADS1(red) and EADS2(green) for the time-resolved decay of W191C CcP with Fe(III) Cc.

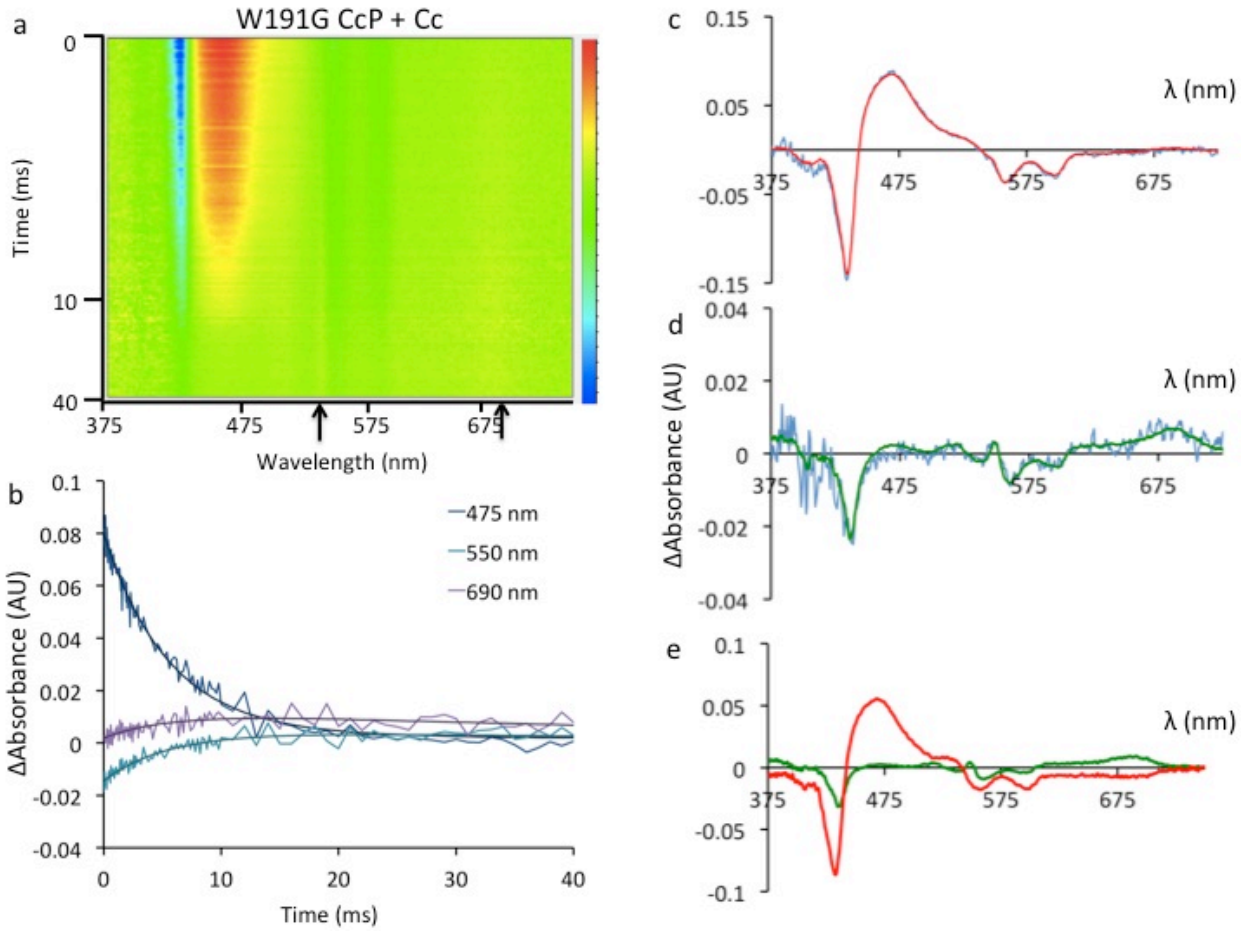

1.4 Discussion

Kinetic scheme for forward electron transfer

As Scheme 3 shows, the rates of ET in solution compete with the binding and dissociation rates between ZnCcP and Cc. The following kinetic analysis will use these symbols as shorthand:

The following are all concentrations:

Zn^* = triplet ZnCcP

Zn_o^* = triplet ZnCcP in complex with Fe(III)Cc

Zn_r^+ = ZnCcP cation in complex with Fe(II)Cc

Zn_r^0 = ZnCcP in complex with Fe(II)Cc

Zn_o^+ = ZnCcP cation in complex with Fe(III)Cc

Zn^0 = Free ZnCcP

Zn^+ = Free ZnCcP cation

C^r = Fe(II)Cc

C^o = Fe(III)Cc

The forward ET reaction is summarized below.

$$Zn^* + C^o \underset{koff}{\overset{kon}{\rightleftarrows}} Zn_o^* \xrightarrow{ke} Zn_r^+$$

Before forward electron transfer can occur, the Zn^*C^O complex must form, although under our conditions the pre-established equilibrium highly favors the complex. The amount of ET active complex is a function of k_{on} and k_{off}, which are known to far exceed the expected rate constants for electron transfer.

$$\mathrm{K} = \frac{k_{on}}{k_{off}} = \frac{\mathrm{Zn}^{*}_{\mathrm{o}}}{\mathrm{Zn}^{*}\mathrm{C}^{\mathrm{o}}} \qquad \textbf{(3)}$$

$$\begin{aligned}
\mathrm{Zn}^{*}_{T} &= \mathrm{Zn}^{*}_{\mathrm{o}} + \mathrm{Zn}^{*} \\
\mathrm{Zn}^{*} &= \mathrm{Zn}^{*}_{\mathrm{o}} / \mathrm{KC}^{\mathrm{o}} \\
\mathrm{Zn}^{*}_{T} &= \mathrm{Zn}^{*}_{\mathrm{o}}(1 + 1/\mathrm{KC}^{\mathrm{o}}) \\
\mathrm{Zn}^{*}_{\mathrm{o}} &= \frac{\mathrm{Zn}^{*}_{T}}{(1 + 1/\mathrm{KC}^{\mathrm{o}})} \qquad \textbf{(4)}
\end{aligned}$$

The rate of formation of the charge-separated state we measured, k^{f}_{obs} , is a function of the rate of forward ET and the concentration of excited ZnCcP in complex with Fe(III) Cc.

$$\frac{\mathrm{dZn}^{+}_{r}}{\mathrm{dt}} = k_{e}\mathrm{Zn}^{*}_{\mathrm{o}}$$

Substituting in the relation for the concentration of the excited state complex, we get that

$$\begin{aligned}
\frac{\mathrm{dZn}^{+}_{r}}{\mathrm{dt}} &= k_{e}\mathrm{Zn}^{*}_{\mathrm{o}} = k_{e}\frac{\mathrm{Zn}^{*}_{T}}{(1 + 1/\mathrm{KC}^{\mathrm{o}})} \\
k^{f}_{obs} &= k_{e}\frac{1}{(1 + 1/\mathrm{KC}^{\mathrm{o}})} \qquad \textbf{(5)}
\end{aligned}$$

From Michaelis-Menten kinetics (Chapter 2), we can approximate K from $1/K_M$ i.e. $\mathrm{K} = 3.3\times10^{4}$ M^{-1} at 300 mM ionic strength, and $C^{O} = 2\times10^{-4}$. With these values in Eqn. 5, $k^{f}_{obs} = 0.86\, k_{e}$. Thus, the true ET rate constants, will be related to the observed

forward rate constants by a factor of 1.16. Despite this, we can see that the driving force dependence holds (Figure 1.11). Because the Cc mutations are far from the binding interface, there should be no steric effects hindering binding of CcP to the Cc mutants. Given the fact that CcP has equal affinity to the reduced and oxidized forms of Cc(Alexander N Volkov et al., 2011), it seems likely that CcP would have equal affinity for all of the Cc variants, most of which maintain the same overall charge. We conclude that the change in forward rates seen with the WT, W191Y, and W191F must be a factor of the driving force.

As the driving force increases, it is usually expected that the rates of forward ET, which happens in a single tunneling step, will increase as well. But in this system, we observe a decrease in ET rates as ZnCcP is paired with higher potential mutants. The observation that Cc species with a potential lower than that of WT display faster kinetics indicates that the energetics of the ZnCcP/Cc interaction lie within the Marcus inverted region.

Figure 1.11. Forward ET Rates of W191F. ET rates of W191F ZnCcP in solution with various mutants of Cc are shown plotted here against the potential of Cc. Forward rate constants are shown in blue, back rate constants are shown in red. Forward rate constants have been adjusted to account for dissociation effects. A decrease in ET rates at the potential increases while the reorganization energy remains constant is evidence of the Marcus inverted region. The back ET rates should not remain constant, indicating that binding kinetics may be affecting the measured rates.

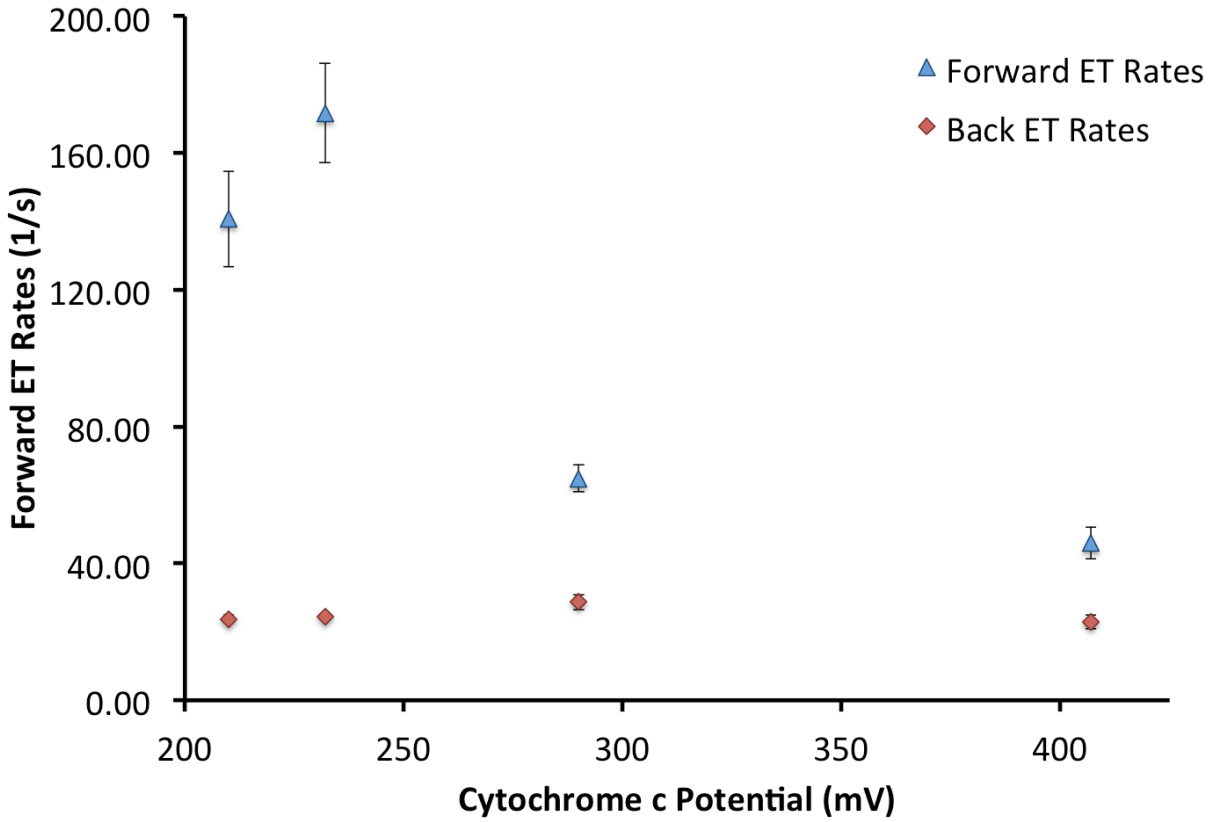

Rates for WT and W191Y ZnCcP

For the wild-type and W191Y CcP, the radical that forms on the W191 or Y191 greatly accelerates the back electron transfer. However, when examining the kinetics, we must consider that the radical can exchange between the W/Y sidechain and the radical.

$$Zn^0 \xleftarrow{keb1} Zn_r^0(W/Y)^+ \underset{kexr}{\overset{kexf}{\rightleftarrows}} Zn_r^+(W/Y)^0 \qquad Zn^0 \xleftarrow{keb2} Zn_r^+(W/Y)^0$$

$$K_{ex} = \frac{k_{exf}}{k_{exr}} = \frac{Zn_r^0(W/Y)^+}{Zn_r^+(W/Y)^0} = e^{F\Delta E/RT} \qquad \textbf{(6)}$$

k_{exf} and k_{exr} are the rate constants of exchange between the ZnPor radical and the W/Y191 radical, and $k_{eb1}$and k_{eb2} are the rates of back ET from Cc through to either the ZnPor$^+$ or the W/Y$^+$ radical. The relation for K_{ex} comes from the Nernst equation, under the conditions that the ET between ZnPor and W/Y191 has reached equilibrium. ΔE represents the difference in reduction potential between ZnPor$^+$ and W/Y191$^+$, F is the Faraday constant, R is the universal gas constant and T is temperature. Because of their close proximity, k_{exf} and k_{exr} are expected to be extremely rapid, much greater than k_{eb}. Since the lack of a hopping site, such as in W191F and W191G greatly slows k_{eb}, we can assume that $k_{eb1} >> k_{eb2}$. Under those assumptions,

$$\frac{dZn^0}{dt} = k_{eb}^1 \, Zn_r^0(W/Y)^+$$

$$\frac{dZn^0}{dt} = k_{eb}^1 \, K_{ex} Zn_r^+(W/Y)^0$$

$$k_{obs} = k_{eb}^1 \, K_{ex} \qquad \textbf{(7)}$$

K_{eb} in the presence of a hopping site remains too fast to be measured, but it is in the range of 10^4 s^{-1}(S. A. Kang & Crane, 2005; S. A. Kang et al., 2006; Seong A Kang et al., 2004). With our measured values of ~10^2 s^{-1} for k_e, this leads to a value of K_{ex} approximately 10^{-2}, indicating that the radical spends most of its time on the porphyrin. This agrees with molecular dynamic simulations that find the radical to be on the sidechain only 2-12% of the time(Beratan, 2013). Using this value for K_{ex} with Eq. 6, we can calculate that $\Delta E \approx 120$ mV.

Back ET Rates for CcP without a hopping site

Because the back ET is quite slow compared to the rates of k_{off}, we have to consider the effects of complex dissociation on the rates we observe (Scheme 2). As mentioned earlier, we estimate that 1-3% of Fe(III) Cc becomes Fe(II) Cc during the reaction, and that non-reactive Fe(III) Cc will compete with Fe(II) Cc for binding of $ZnCcP^+$, prolonging the charge separated state. For back ET to occur, the charge-separated elements must first form a complex.

$$\frac{\mathrm{dZn}^0}{\mathrm{dt}} = k_{on}\mathrm{Zn}^+\mathrm{C}^r$$

$$\mathrm{K} = \frac{k_{on}}{k_{off}} = \frac{\mathrm{Zn}^0_r}{\mathrm{Zn}^0\mathrm{C}^r} = \frac{\mathrm{Zn}^+_{\mathrm{o}}}{\mathrm{Zn}^+\mathrm{C}^{\mathrm{o}}} \qquad \textbf{(8)}$$

The fraction of $ZnCcP^+$ and Fe(II) Cc not bound to each other are functions of the equilibrium constant K, which we assume is the same regardless of the ZnCcP and Cc oxidation states.

$$\begin{aligned}
\mathrm{Zn}^+_T &= \mathrm{Zn}^+_{\mathrm{o}} + \mathrm{Zn}^+ \\
\mathrm{Zn}^+_{\mathrm{o}} &= \mathrm{Zn}^+\mathrm{KC}^{\mathrm{o}} \\
\mathrm{Zn}^+_T &= \mathrm{Zn}^+(1+\mathrm{KC}^{\mathrm{o}}) \\
\mathrm{Zn}^+ &= \frac{\mathrm{Zn}^+_T}{(1+\mathrm{KC}^{\mathrm{o}})} \qquad \textbf{(9)}
\end{aligned}$$

$$\begin{aligned}
\mathrm{C}^r_T &= \mathrm{C}^r + \mathrm{Zn}^0_r \\
\mathrm{C}^r_T &= \mathrm{C}^r(1+\mathrm{KZn}^0) \\
\mathrm{C}^r &= \frac{\mathrm{C}^r_T}{(1+\mathrm{KZn}^0)} \qquad \textbf{(10)}
\end{aligned}$$

Substituting these expressions into our equation for the rate of complex formation, we find that

$$\frac{\mathrm{dZn}^0}{\mathrm{dt}} = k_{on}\mathrm{Zn}^{+}\mathrm{C}^{r} = k_{on}\frac{\mathrm{Zn}_T^{+}}{(1+\mathrm{KC}^{o})}\frac{\mathrm{C}_T^{r}}{(1+\mathrm{KZn}^0)}$$

Because the return to ground state is dependent on the concentration of the intermediate state, we know that

$$\frac{\mathrm{dZn}^0}{\mathrm{dt}} = k_{obs}^{b}\mathrm{C}_T^{r}$$

$$\frac{\mathrm{dZn}^0}{\mathrm{dt}} = k_{on}\frac{\mathrm{Zn}_T^{+}}{(1+\mathrm{KC}^{o})}\frac{1}{(1+\mathrm{KZn}^0)}\mathrm{C}_T^{r}$$

$$k_{obs}^{b} = k_{on}\frac{\mathrm{Zn}_T^{+}}{(1+\mathrm{KC}^{o})}\frac{1}{(1+\mathrm{KZn}^0)} \qquad \textbf{(11)}$$

Using $K = 3.3{\times}10^4$ from the Michaelis-Menten measurements, $Zn_T^{+} \approx 0.01 * Zn_T = 10^{-6}$, and $k_{on} \approx 10^8\ \mathrm{s}^{-1}$, we get $k_{obs}^{b} \approx 4\ \mathrm{s}^{-1}$. Although the rates we measure are an order of magnitude higher, around 30 s^{-1} , we do not observe a dependence on driving force, as this equation predicts. Thus, because the data was taken at high ionic strength, the binding kinetics likely dominate the measurement.

Ionic Strength Dependence

To test this the ionic strength dependence, rates were measured at a range of ionic strengths, from 30 to 420 mM KPi (Table 1). At the highest ionic strength, as salt ions screen the complex from binding, both the forward and back ET rates become very slow, about 20% of their value at 100 mM KPi. It has been shown that higher salt

concentrations lead to a decreased K (Mei et al., 1996), and that would explain the behavior seen in the kinetics. The formation of EADS2 increases with time and little decrease is observed in the time period monitored, indicating that after reduction, Fe(II) Cc and ZnPor+CcP remain dissociated for a long period of time.

Forward ET behavior is similar at the lower ionic strength of 30 mM KPi. The forward rates display an inverted relationship with the driving force. However, back ET rates also demonstrate an inverted effect, with the back ET rates scaling proportionally with Cc mutant potential. The highest potential Cc mutant, Y48K, has a back ET rate 34% greater than that of the lowest potential mutant, Y48H, despite having a driving force that is 197 mV less. At higher ionic strength this is not observed because dissociation of the complex competes with ET rates.

At the lower ionic strength of 30 mM KPi, ET rates are significantly higher. Measurements with Y48H show forward ET rates 1.4 times larger and back ET rates 2.5 times larger. For Y48K, the highest potential mutant, forward rates become a surprising 6 times larger and back rates 3 times larger. The low salt concentration would lead to a longer complex lifetime and more frequent complex formation. It is unexpected, however, that the rates for Y48K Cc would be greater than that for Y48H Cc at low ionic strength when the reverse is true at higher ionic strength. Although there is a second binding site that has higher activity but lower affinity (Alexander N Volkov et al., 2011) that is present at lower salt concentrations, it should still be subject to the driving force

dependence. The cause of the discrepancy in the forward rates is unknown and will need to be investigated through further measurement.

The inverted effect is also observed in back ET rates at the lower ionic strength. At this lower ionic strength, the binding constant K will be high and k_{eb} will reflect the rate of ET and not complex formation. Back ET from Y48H (E^0 = 210 mV) is measured at 49.58 ± 2.1 s^{-1}, and 65.49 ± 7.3 s^{-1} from Y48K (E^0 = 407 mV). The higher E0 of Y48K creates a lower driving force in sending an electron to the porphyrin cation, but the rate observed is higher. This negative correlation with driving force indicates that superexchange ET from Cc to $ZnPor^+$ is in the inverted region.

Calculation of reorganization energy and electronic coupling

The mutations in Cc and CcP have given us the opportunity to alter ΔG while keeping the donor-acceptor distance the same. The rates should follow the non-adiabatic, high temperature rate equation:

$$k_{ET} = \frac{2\pi}{\hbar}\frac{1}{\sqrt{4\pi\lambda k_B T}}\langle H_{DA}^2\rangle e^{-\frac{(\Delta G+\lambda)^2}{4\lambda k_B T}} \qquad \textbf{(12)}$$

Fitting the forward ET rates measured, adjusted for the effects of Cc dissociation, to this equation, we get the following values for reorganization energy and electronic coupling (Table 2).

CcP*	HDA (10^-14 ev^2)	lambda (eV)
WT	0.8301	0.77
W191Y	1.118	0.80
W191F	0.9040	0.72
W191F (30 mM KPi)	1.442	0.98

* In 100 mM KPi unless noted

Table 1.2: Coupling constants and reorganization energies calculated from forward electron transfer rates.

These compare favorably to coupling constants and reorganization energies previously calculated (Mei et al., 1996). As all the mutations present in this study have little impact on the geometry of the zinc or iron coordination, it's likely that the reorganization energy is the same for all pairings of WT, W191Y, and W191F CcP to the four species of Cc. The true reorganization energy is somewhere in the range reported here. As shown in Figure 1.12, the fit supports our conclusion that the rates measured are in the inverted region. For forward ET from ZnCcP to Cc, the lower potential mutants (Y48H and N52I) are quite near the optimal driving force, whereas WT Cc and Y48K have a driving force greater than the reorganization energy.

It is interesting that the calculated reorganization energy would alter with buffer concentration. At lower salt, the complex lifetime should be longer, and the rates measured are greater for both forward and back ET. The inverted effect is still observed. However, the higher reorganization energy suggests that the ET is optimized for a higher driving force in the more stable complex. This system can be used in future studies to elucidate the role of solvent interactions on the reorganization energy of protein complexes.

Kinetics of W191G ZnCcP

Since ZnW191G CcP lacks a hopping site, the kinetics were expected to behave like W191F. Indeed, we are able to observe an intermediate charge-separated state. However, the forward ET rates measured are faster in W191G than W191F (72 s^{-1} compared to 56 s^{-1}), and back rates are slower (16 s^{-1} compared to 28 s^{-1}). For the back rates, the likely explanation is that the W191G mutation caused the loop from residues 190 to 195 to become flexible, allowing a hinge-like motion in solution. While structures show that this does not prevent formation of the active complex (Chapter 2), it may delay formation, as now CcP must sample additional conformations.

The faster forward ET rate is more difficult to explain. There is evidence that the W191G mutation disturbs the electronic state of the CcP cofactor more than W191F. The Soret peak of FeW191G resides at 414 nm, while WT, W191Y, and W191F CcP show a Soret peak at 409 nm (Chapter 2). The ZnCcP spectra is also slightly perturbed, with the WT, W191Y, and W191F Soret peaks at 432 nm (Figure 1.3) and W191G having a Soret peak at 430 nm (not shown). Although minor shifts, these indicate that the lost of the sidechain at residue 191 perturbs the electronic environment. This could alter the driving force and lead to the higher ET rates observed.

Comparison to Published Rates

The kinetic models presented here are consistent with previously published ZnCcP/Cc kinetic schemes, and we are confident that the species attributed to the spectral changes observed are correct. However, our rate constants do not agree with all published rates. The rates measured for the triplet state decay of ZnCcP,k_{zn}, alone agree very well with the published rates, which usually falls between 100 – 120 s^{-1}(Ho et al., 1985; S. A. Kang & Crane, 2005; S. A. Kang et al., 2006; Seong A Kang et al., 2004; Seifert et al., 2005). However, the rates of forward ET are lower than previously published. Forward ET from various CcP mutants usually falls around 220 s-1, both in solution (Seifert et al., 2005) and in crystals (Seong A Kang et al., 2004). Correcting for dissociation of Cc in the high-salt solution does not reconcile these rates.

The measured solution rates were done at much lower protein concentrations, typically in the 5 – 10 μM range, whereas the studies presented here are at 100 μM CcP. It may be that the crowding effect caused by high concentrations leads to less conformational flexibility in the two proteins, making it more difficult for them to access the ET active conformation.

Conclusions

The coupling constant and the reorganization energy have remained understudied. It is our hope that the scheme we have presented of varying the driving force can be

adapted to other systems, like photosynthesis and respiration, to better understand the energetics of these essential ET processes. And in general, we hope to better understand how the protein environment tunes the reorganization energy of the various cofactors found in nature.

Our measurement of the reorganization energy is one of the first in a biologically relevant system. While we believe there is an optimum ET-active conformation of the complex between CcP and Cc, in solution the two proteins would be sampling a large range of conformations, and the rates measured are likely an average of that. The effect of salt concentration in solution on the complex lifetime and reorganization energy has been demonstrated as an important factor that requires more investigation. Ideally, these measurements will be performable on crystals of the complex, and the rates of ET in a static complex can be measured. Despite this, because our measurements are based on the comparison of nearly identical proteins with different driving forces, we believe the rates accurately reflect perturbation to the Marcus parameters.

In this work, we have presented the compete time-dependent UV/Vis spectra of the excited triplet state on the microsecond timescale. We were able to directly observe the reduction and subsequent oxidation of Cc by CcP through spectral changes, and calculate the rates of ET. In addition, we have presented a scheme for the measurement of the reorganization energy in the electron transfer between two proteins by varying the driving force. Ourresults establish that these ET reactions ovvucr within

the inverted regime of the Marcus curve, in good agreement with theoretical calculations on this system.

1.5 Bibliography

Beratan, Nan Jiang; Aleksey Kuznetsov; Judith M. Nocek; Brian M. Hoffman; Brian R. Crane; Xiangqian Hua; David N. (2013). Compensating changes in tunneling interactions and reor-ganization energies explain the apparent distance-independent charge recombination kinetics in cytochrome c - cytochrome c peroxidase complexes. *Unpublished*.

Bjerrum, Morten J, Casimiro, Danilo R, Chang, I-Jy, Di Bilio, Angel J, Gray, Harry B, Hill, Michael G, . . . Winkler, Jay R. (1995). Electron transfer in ruthenium-modified proteins. *Journal of bioenergetics and biomembranes, 27*(3), 295-302.

Burda, Květoslava. (2007). Dynamics of electron transfer in photosystem II. *Cell biochemistry and biophysics, 47*(2), 271-284.

Chae Hee Kang, Shelagn Ferguson-Miller, and E. Margoliash. (1977). Steady State Kinetics and Binding of Euakryotic Cytochromes c with Yeast Cytochrome c Peroxidase. *J Biol Chem, 252*(3), 919-926.

Hays Putnam, A. M., Lee, Y. T., & Goodin, D. B. (2009). Replacement of an electron transfer pathway in cytochrome c peroxidase with a surrogate peptide. *Biochemistry, 48*(1), 1-3. doi: 10.1021/bi8020263

Ho, Pui Shing, Sutoris, Carol, Liang, Nong, Margoliash, E, & Hoffman, Brian M. (1985). Species specificity of long-range electron transfer within the complex between zinc-substituted cytochrome c peroxidase and cytochrome c. *J Am Chem Soc, 107*(4), 1070-1071.

Hong, Jing, Kharenko, Olesya A, Fan, Jiufeng, Xie, Fei, Petros, Amy K, Gibney, Brian R, & Ogawa, Michael Y. (2006). Evidence that a miniature CuI metalloprotein undergoes collisional electron transfer in the inverted Marcus region. *Angewandte Chemie International Edition, 45*(37), 6137-6140.

Kang, S. A., & Crane, B. R. (2005). Effects of interface mutations on association modes and electron-transfer rates between proteins. *Proc Natl Acad Sci U S A, 102*(43), 15465-15470. doi: 10.1073/pnas.0505176102

Kang, S. A., Hoke, K. R., & Crane, B. R. (2006). Solvent isotope effects on interfacial protein electron transfer in crystals and electrode films. *J Am Chem Soc, 128*(7), 2346-2355. doi: 10.1021/ja0557482

Kang, Seong A, Marjavaara, Pieti J, & Crane, Brian R. (2004). Electron transfer between cytochrome c and cytochome c peroxidase in single crystals. *J Am Chem Soc, 126*(35), 10836-10837.

Koloczek, H, Horie, T, Yonetani, T, Anni, H, Maniara, G, & Vanderkooi, JM. (1987). Interaction between cytochrome c and cytochrome c peroxidase: excited-state reactions of zinc-and tin-substituted derivatives. *Biochemistry, 26*(11), 3142-3148.

Lett, C Marc, & Guillemette, J Guy. (2002). Increasing the redox potential of isoform 1 of yeast cytochrome c through the modification of select haem interactions. *Biochemical Journal, 362*(Pt 2), 281.

Marcus, R Al, & Sutin, Norman. (1985). Electron transfers in chemistry and biology. *Biochim Biophys Acta, 811*(3), 265-322.

Mei, Hongkang, Wang, Kefei, McKee, Stacey, Wang, Xuming, Waldner, Jennifer L, Pielak, Gary J, . . . Millett, Francis. (1996). Control of formation and dissociation of the high-affinity complex between cytochrome c and cytochrome c peroxidase by ionic strength and the low-affinity binding site. *Biochemistry, 35*(49), 15800-15806.

Miller, JR, Calcaterra, LT, & Closs, GL. (1984). Intramolecular long-distance electron transfer in radical anions. The effects of free energy and solvent on the reaction rates. *J Am Chem Soc, 106*(10), 3047-3049.

Miller, M. A. (1996). A complete mechanism for steady-state oxidation of yeast cytochrome c by yeast cytochrome c peroxidase. *Biochemistry, 35*(49), 15791-15799. doi: 10.1021/bi961488c

Nocek, Judith M, Stemp, Eric DA, Finnegan, Michael G, Koshy, Thomas I, Johnson, Michael K, Margoliash, E, . . . Hoffman, Brian M. (1991). Low-temperature, cooperative conformational transition within [Zn-cytochrome c peroxidase, cytochrome c] complexes: Variation with cytochrome. *J Am Chem Soc, 113*(18), 6822-6831.

Page, Christopher C, Moser, Christopher C, Chen, Xiaoxi, & Dutton, P Leslie. (1999). Natural engineering principles of electron tunnelling in biological oxidation–reduction. *Nature, 402*(6757), 47-52.

Panavas, Tadas, Sanders, Carsten, & Butt, Tauseef R. (2009). SUMO fusion technology for enhanced protein production in prokaryotic and eukaryotic expression systems *SUMO Protocols* (pp. 303-317): Springer.

Pearl, Naw May, Jacobson, Timothy, Arisa, Moraa, Vitello, Lidia B, & Erman, James E. (2007). Effect of single-site charge-reversal mutations on the catalytic properties of yeast cytochrome c peroxidase: mutations near the high-affinity cytochrome c binding site. *Biochemistry, 46*(28), 8263-8272.

Pelletier, Huguette, & Kraut, Joseph. (1992). Crystal structure of a complex between electron transfer partners, cytochrome c peroxidase and cytochrome c. *Science, 258*(5089), 1748-1755.

Pollock, W Brent R, Rosell, Federico I, Twitchett, Mark B, Dumont, Mark E, & Mauk, A Grant. (1998). Bacterial expression of a mitochondrial cytochrome c. Trimethylation of Lys72 in yeast iso-1-cytochrome c and the alkaline conformational transition. *Biochemistry, 37*(17), 6124-6131.

Seifert, J. L., Pfister, T. D., Nocek, J. M., Lu, Y., & Hoffman, B. M. (2005). Hopping in the electron-transfer photocycle of the 1:1 complex of Zn-cytochrome c

peroxidase with cytochrome c. *J Am Chem Soc, 127*(16), 5750-5751. doi: 10.1021/ja042459p
Snellenburg, Joris J, Laptenok, Sergey P, Seger, Ralf, Mullen, Katharine M, & van Stokkum, Ivo HM. (2012). Glotaran: A Java-Based Graphical User Interface for the R Package TIMP. *J. Stat. Softw, 49*, 1-22.
van Stokkum, Ivo HM, Larsen, Delmar S, & van Grondelle, Rienk. (2004). Global and target analysis of time-resolved spectra. *Biochimica et Biophysica Acta (BBA)-Bioenergetics, 1657*(2), 82-104.
Volkov, A. N., Bashir, Q., Worrall, J. A., & Ubbink, M. (2009). Binding hot spot in the weak protein complex of physiological redox partners yeast cytochrome C and cytochrome C peroxidase. *J Mol Biol, 385*(3), 1003-1013. doi: 10.1016/j.jmb.2008.10.091
Volkov, Alexander N, Nicholls, Peter, & Worrall, Jonathan AR. (2011). The complex of cytochrome< i> c</i> and cytochrome< i> c</i> peroxidase: The end of the road? *Biochimica et Biophysica Acta (BBA)-Bioenergetics, 1807*(11), 1482-1503.
Volkov, Alexander N, Worrall, Jonathan AR, Holtzmann, Elodie, & Ubbink, Marcellus. (2006). Solution structure and dynamics of the complex between cytochrome c and cytochrome c peroxidase determined by paramagnetic NMR. *Proceedings of the National Academy of Sciences, 103*(50), 18945-18950.
Wang, Kefei, Mei, Hongkang, Geren, Lois, Miller, Mark A, Saunders, Aleister, Wang, Xuming, . . . Millett, Francis. (1996). Design of a ruthenium-cytochrome c derivative to measure electron transfer to the radical cation and oxyferryl heme in cytochrome c peroxidase. *Biochemistry, 35*(47), 15107-15119.
Yonetani, Takashi. (1967). Studies on cytochrome c peroxidase X. Crystalline apo-and reconstituted holoenzymes. *Journal of Biological Chemistry, 242*(21), 5008-5013.

Chapter 2

Crystallographic Studies on the Hopping Site of Cytochrome c Peroxidase

1. Introduction

Reduction and oxidation reactions in biological systems often involve electron transfer (ET) occurring over 10s of Å of distance(Cordes & Giese, 2009). Electrons can be thought to tunnel between overlapping orbitals of the donor and acceptor molecules, in a process known as superexchange(Cordes et al., 2008). There has been considerable debate over whether ET in proteins occurs via superexchange between cofactors, or is mediated by a bridge involving the intervening protein. Gray and Winkler have done multiple studies of ET with photo-excitable ruthenium tags attached to small redox proteins like azurin and cytochrome c, and have shown that the rates of ET between the tags and metal centers can be modeled as a single-tunneling step with an exponential distance dependence(Gray & Winkler, 2003). Efficient ET has not been measured at distances greater than 20Å, which may represent the maximum effective distance for a single tunneling step. In studies of structures of known redox proteins, Dutton et. Al. have found that cofactors are rarely spaced more than 14 Å apart, and he places the cut-off there (Page, Moser, Chen, & Dutton, 1999). Indeed, in protein complexes where electrons are moved great distances, cofactors tend to be found spaced closely together. In mitochondrial respiration, charges move from flavins to quinones to iron-sulfur clusters and on to hemes, all of which are spaced 8 – 14 Å apart(Rich, 2003). Photosystem II, part of the protein network responsible for photosynthesis, sends an

electron through a pheophytin, two quinones and a heme to the oxidized chlorophyll at the end (Burda, 2007). Although the peptide bonds between the cofactors surely influence tunneling rates, the way nature has placed cofactors would argue that super-exchange is the dominant mechanism of ET.

However, to transfer electrons over distances longer than 14 Å an intermediate is needed between cofactors, and a redox active amino acid can fill that role. In many redox proteins, an oxidized tyrosine or tryptophan has been detected during long range ET. The formation of tryptophan radicals is a common feature in the reaction mechanisms of peroxidases (Jasion, Doukov, Pineda, Li, & Poulos, 2012) (Shih et al., 2008). The mechanism of ribonucleotide reductase involves at least three tyrosines and a tryptophan across 30 Å and two peptide chains (Seyedsayamdost, Xie, Chan, Schultz, & Stubbe, 2007). DNA Photolyase, a light-induced flavoprotein that repairs thymine dimers, oxidizes three tryptophans sequentially in order to separate the nucleotides (Lukacs, Eker, Byrdin, Brettel, & Vos, 2008). Studies on rates of ET across a 20Å artificial helical peptide have shown that introduction of an aromatic residue halfway between donor and acceptor increased rates of ET 30-fold, and an oxidized intermediate was spectroscopically identified(Cordes et al., 2008; Giese et al., 2005).

As described in Chapter 1, the mechanism for oxidation of Fe(II) Cc involves the formation of a stable radical on W191. It is well established that in the natural reaction cycle this radical site is reduced by Cc and that the oxyferryl is reduced subsequently by

a second molecule of Cc. More recently it has been suggested that the Trp acts as an electron hopping site in the photochemically driven recombination reaction of ZnPorCcP with Cc. Mutagenesis studies have shown that mutation of W191 to phenylalanine (Seifert, Pfister, Nocek, Lu, & Hoffman, 2005) results in loss of peroxidase activity and leads to slower ET rates between Cc and ZnCcP. It has also been shown that the W191G mutation leads to loss of activity and creates a cavity where aromatic compounds can bind(Fitzgerald, Churchill, McRee, & Goodin, 1994). In this chapter we present the structures of these mutants in complex with Cc, and attempt to characterize the nature of an active hopping site.

Some general properties of hopping sites have been predicted. The redox potential should be greater than the donor but no more than 200 mV higher than the acceptor(Shih et al., 2008). Sidechains that do not occur in nature, such as trimethoxy-substituted phenylalanine, can act as a hopping site when bound to the peptide(Cordes & Giese, 2009). Questions that remain unanswered include if these potential restrictions apply to interprotein electron transfer, and if being bound to the peptide backbone is a necessary requirement.

2. Methods

Crystallography

For mutagenesis and protein purification methods, see Chapter 1. Prior to crystallization, CcP and Cc were combined in a 1-to-1 ratio at a final concentration of 1 mM each. The protein mixture was dialyzed against H_2O overnight to reduce ionic strength and thereby increase CcP/Cc binding. Initial crystal hits were obtained using the Phoenix robot (Art Robbins Instruments, housed in Chris Fromme's lab of the Weill Institute of Cell and Molecular Biology). Larger crystals were grown by vapor diffusion in either sitting or hanging drop trays against a reservoir contains 15 – 25% polyethylene glycol 3350, 175 mM NaCl, and 100 mM sodium acetate, pH 4.8 – 5.6. In some cases, streak seeding was used to increase crystal quality. The crystals formed as thin red blades (Figure 2.1).

Structure Determination

Data was collected at the Cornell High Energy Synchrotron Source (CHESS) at beamlines A1 and F2 on a ADSC Quantum 210 CCD. A mixture of 4 parts reservoir and 1 part ethylene glycol was used as a cryoprotectant for crystals. In soaking experiments with W191G CcP crystals, we followed the protocol described by Goodin et. Al. (Rabi A. Musah, 2002). Briefly, potential small-molecule ligands were dissolved in 50% ethanol to make a 100 mM stock solution, with the exception of indole, which was dissolved in 100% ethanol. The crystals were soaked in a drop of well solution with a final concentration of 30 mM ligand for 30 seconds prior to soaking with cryoprotectant. All data was indexed and scaled with HKL2000 (Otwinowski & Minor,

1997). All structures were phased using molecular replacement in PHENIX (Adams et al., 2010). Structures of W191G CcP were refined using CNS (Brunger et al., 1998) and all other structures were refined with the PHENIX suite. Building and adjustments were made using COOT (Emsley & Cowtan, 2004). Statistics are reported in Table 2.1.

Figure 2.1: Crystals of CcP/Cc complex. a) Initial hits were formed in a robot tray drop. b) Scaled up hanging drop crystals from the same conditions as the robot tray. c) Highest quality crystals, obtained by seeding from the crystals in b). d) Close-up of the crystals in c). The blades are about 200 µm in length and 10 µM in thickness.

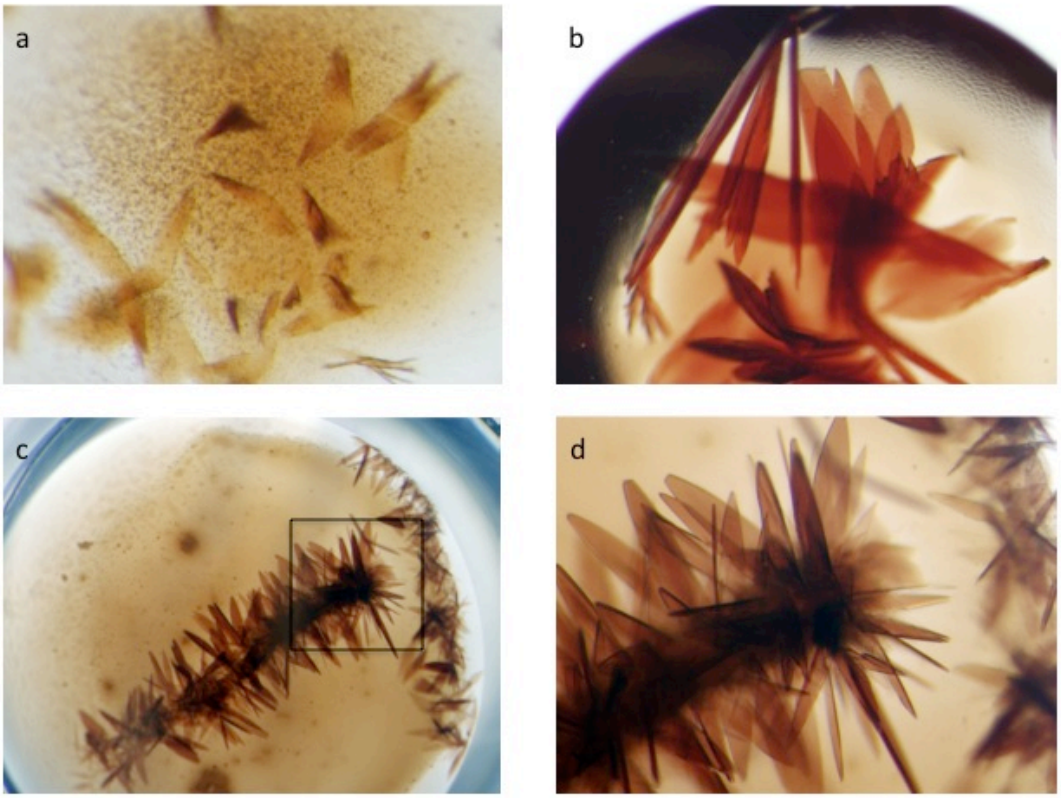

Table 2.1: Structure Statistics

	W191F	W191Y	W191G	W191G + Aniline
Data Collection				
Space group	P 2_1	P 2_1	P 2_1	P 2_1
a, b, c (Å)	44.8, 113.8, 88.2	45.2, 110.4, 88.0	45.4, 117.1, 88.9	45.4, 110.3, 87.9
α, β, γ	90, 105.3, 90	90, 104.8, 90	90, 105.1, 90	90, 105.5, 90
Unique reflections	51802	32055	52487	27836
Resolution (Å)	2.0	2.4	2.06	2.5
Last shell (Å)	2.03 – 2.0	2.44 – 2.40	2.13 - 2.06	2.54 – 2.5
Redundancy (overall/last shell)	3.3/3./0	3.7/3.2	2.9/2.7	3.1/2.6
Completeness (%/last shell)	91.3/82.5	97.3/87.5	94.91/86.09	94.3/79.7
I/σ (overall/last shell)	6.45/3.81	52.7/4.0	6.86/2.65	5.39/2.04
Linear R-fac (R_{merge}) (overall/last shell)	0.222/0.488	0.130/0.401	0.121/0.46	0.158/0.537
Refinement				
R_{work} (%)	0.216	0.2442	0.237	0.256
R_{free} (%)	0.278	0.3025	0.263	0.311
No. atoms	6952	6664	6773	5763
No. water molecules	434	146	185	65
Mean B value	31.8	51.3	44.30	76.1
B value (waters)	30.4	41.1	41.70	60.4
B value (ligands/ions)	22.6	45.9	47.90	41.9
RMSD from ideal bond lengths (Å)	0.008	0.004	0.005	0.003
RMSD from ideal bond angles (°)	1.18	1.3	1.0	0.83
Ramachandran statistics (%)				
Most favored	97.0	94.0	96.0	95.0
Disallowed	0.13	1.3	0.38	1.0

Table 2.1 Continued

	W191G + o-Toluidine	W191G + 24dma	W191G + 3abt
Data Collection			
Space group	P 2_1	P 2_1	P 2_1
a, b, c (Å)	45.4, 111.9, 87.9	45.4, 107.5, 87.2	45.3, 117.5, 88.5
α, β, γ	90, 104.3, 90	90, 104.5, 90	90, 104.4, 90
Unique reflections	20359	15317	51366
Resolution (Å)	2.75	3.0	2.10
Last shell (Å)	2.59 - 2.55	3.05 – 3.00	2.14 – 2.10
Redundancy (overall/last shell)	5.4/4.4	8.4/7.3	7.0/6.5
Completeness (%/last shell)	93.02/62.64	95.2/85.0	98.7/90.0
I/σ (overall/last shell)	13.99/3.24	17.2/3.4	14.2/4.7
Linear R-fac (R_{merge}) (overall/last shell)	0.092/0.388	0.123/0.512	0.096/0.402
Refinement			
R_{work} (%)	0.218	0.242	0.218
R_{free} (%)	0.268	0.320	0.265
No. atoms	6597	6588	7084
No. water molecules	9	0	496
Mean B value	76.9	86.4	45.0
B value (waters)	39.9	NA	46.7
B value (ligands/ions)	82.2	24.2	24.2
RMSD from ideal bond lengths (Å)	0.004	0.008	0.004
RMSD from ideal bond angles (°)	0.89	0.82	0.74
Ramachandran statistics (%)			
Most favored	95	92.0	98.0
Disallowed	0.13	0.63	0.0

Michaelis-Menten Kinetics

The steady-state assay for CcP activity was carried out as previously described (Chae Hee Kang, 1977). Stock solutions of Cc were reduced on ice in the glovebox by incubating with 10 mM DTT for one hour. DTT was then removed by buffer exchange into 100 mM KPi pH 7.0, either by PD-10 desalting columns or ten rounds of concentration and dilution using Millipore Amicon Ultra centrifugal filters (10 kDa cutoff). Samples containing 2 nM peroxidase, 100 mM KPi pH 6.0, and 0 – 75 uM Cc were then prepared anaerobically to a volume of 1800 µL in gastight cuvettes(StarnaCell). Samples were placed in a Hewlett Packard 8909A peltier sample cooler kept at 24 C and stirred at 500 RPM. Spectra were taken with an Agilent 8453 Spectrophotometer. Samples were blanked prior to data acquisition to monitor the change in absorbance over time.

The reaction was initiated by addition of hydrogen peroxide to a final concentration of 170 µM. Oxidation of Cc was monitored at 550 nm and 540 nm. Absorbance at 750 nm was also monitored as a baseline that should remain constant over the course of the reaction. The kinetics were monitored for 60 s, with data collected every 0.5 seconds. The data was then baseline corrected and plotted in Microsoft Excel. The initial range of data where the reaction progress is linear was chosen to represent the steady-state progress of the reaction, where Cc concentration greatly exceeded enzyme concentration. A linear fit was applied to this range and the slope was taken as the

reaction velocity (v_0) for that concentration. For every concentration of Cc, three samples were measured.

For measuring the effect of potential ligands on CcP activity, stock solutions of the ligands were prepared in 50% ethanol, or 100% ethanol in the case of indole. Samples were prepared as above, with a Cc concentration of 30 μM and with the addition of ligand stock solution to bring the ligand concentration to 2 mM.

To determine the Michaelis-Menten constants V_{max} and K_m, the average v_0 was plotted vs concentration and fit to the equation $v = \frac{V_{max}[Cc]}{K_M + [Cc]}$ in Mathematica(English et al., 2005). Steady state parameters of W191G with ligands were compared to those of W191F with ligands to identify any non-specific effects not attributable to cavity binding.

Compound 1 Detection

For UV/Vis spectroscopy, 30 μM CcP was prepared in 100 mM KPi, pH 6.0, and hydrogen peroxide was added to a final concentration of 1 mM. Spectra were taken on an Agilent 8453 Spectrophotometer.

For continuous wave EPR, CcP was prepared at a higher concentration to obtain a strong signal. The concentrations varied from sample to sample and are 0.68 (0.74) mM for WT CcP in H_2O (D_2O); 0.57 (0.58) mM for W191Y CcP; 0.47 (0.33) mM for

W191G CcP. For deuterium exchange, protein was dialyzed with Slide-a-Lyzer 7 kDa (Pierce) cassettes into two changes of 100 mM KPi, pH 6.0 D2O buffer, over two days. Prior to data collection, samples were diluted into a buffer of 100 mM KPi, pH 6.0, 2 mM hydrogen peroxide, and 30% glycerol. Samples were loaded into EPR tubes and flash frozen minutes after addition of hydrogen peroxide, and measured with a Bruker EleXSys II spectrometer at 9 GHz and 50 K with 1.5 Gauss modulation frequency and 25 - 30 dB modulation amplitude.

3. Results

Structure of W191X CcP

The structures of W191Y, W191F, and W191G CcP in complex with Fe(III)Cc were determined at resolutions that ranged from 2.0 – 2.4 Å, and are shown overlayed with the wild-type structure in Figure 2.2. All of the CcP mutants form complexes with Cc that are very similar to that formed by the wild-type (WT).

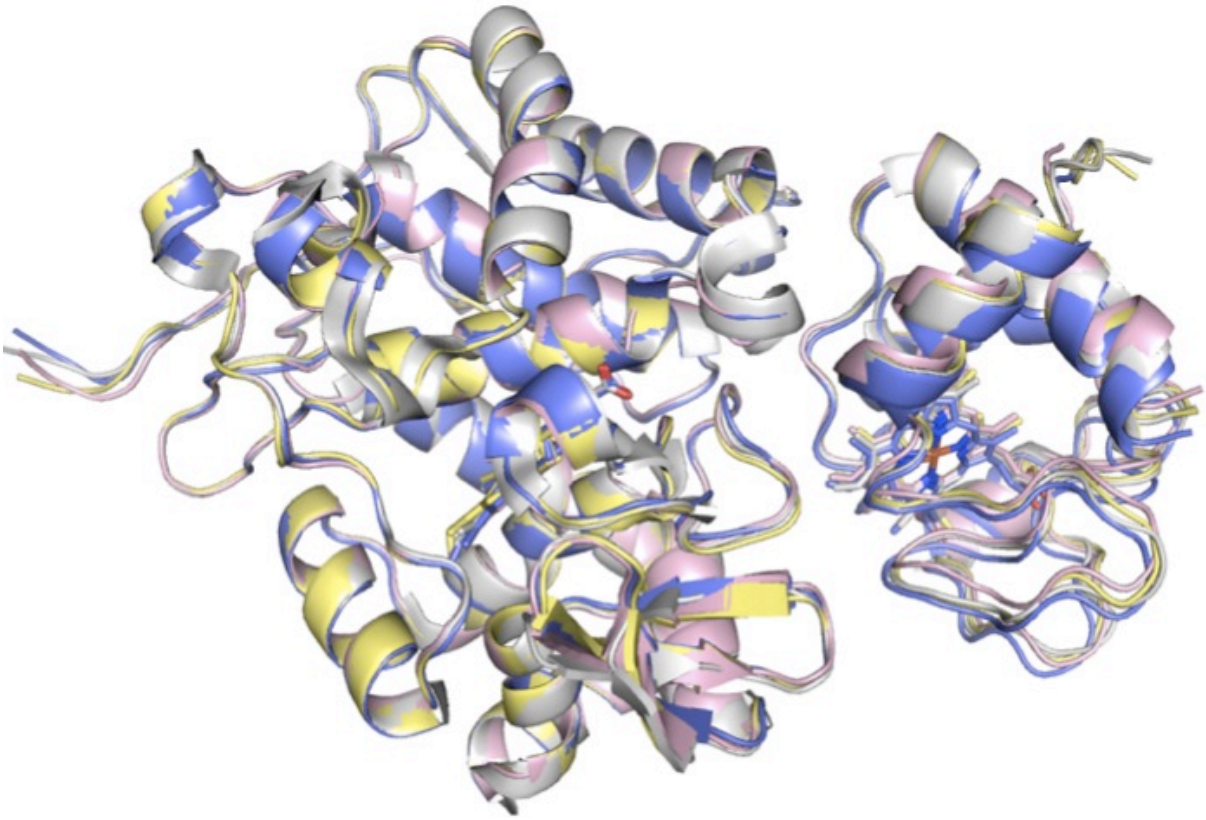

Figure 2.2: Complex Conformation of CcP Mutants with Cc. Overlay of the structures of the complexes of CcP with Cc indicates that the mutations do not prevent formation of the wild-type complex. WT (1U74) is shown in while, W191Y in pink, W191F in blue, and W191G in yellow. Each unit cell has two copies of CcP and Cc. Shown are the A and B chains from each structure.

For each of the mutants, both CcP and Cc retain nearly identical conformations to those seen in the WT complex. It has been previously shown that the W191G mutation causes the loop composed of residues 190 - 195 to become very flexible in the absence of Cc(Melissa M. Fitzgerald, 1996). As this loop is at the binding interface with Cc, there was concern that increased flexibility would impact the formation of the crystal complex. Nonetheless W191G binds Cc in the expected position with each protein in the WT conformation. Each unit cell has two copies of CcP (chains A and C) and two copies of

Cc (chains B and D). Only chains A and B are shown in the figures, but chains C and D display the same conformation.

In the structures of W191Y and W191F, the altered sidechains occupy the same position as W191 in the wild type (Figure 2.3).

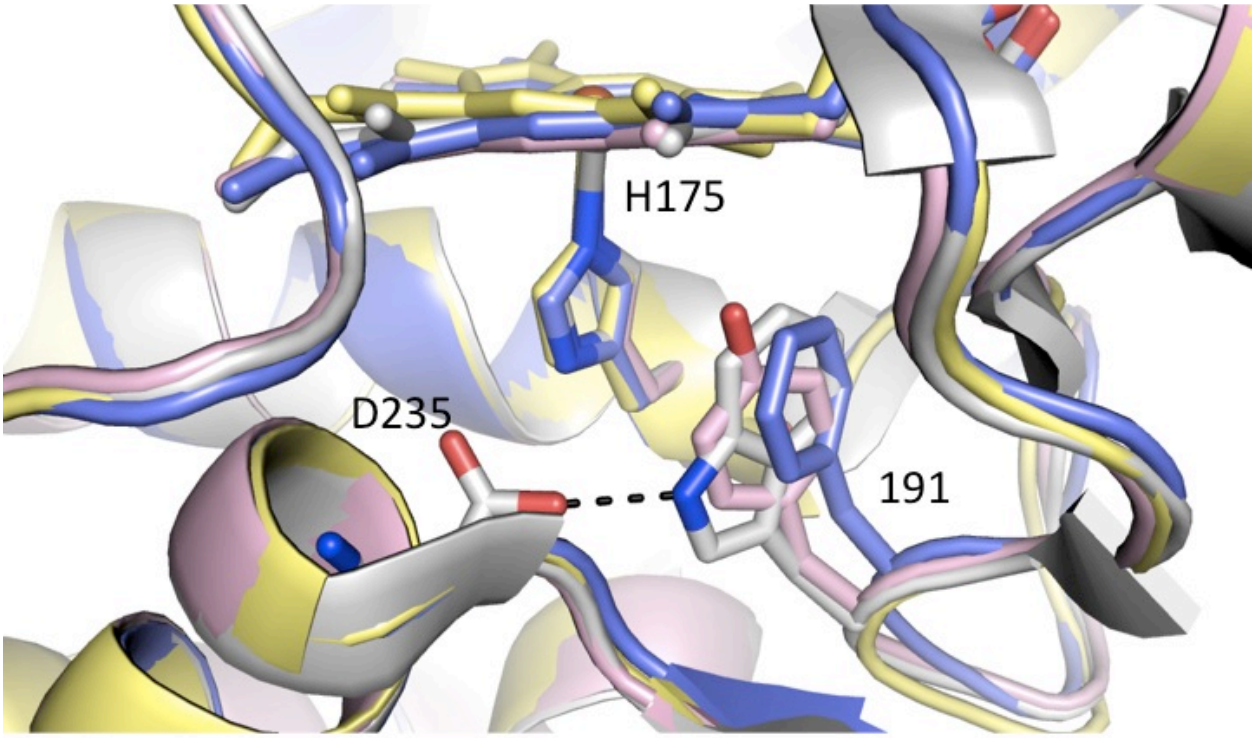

Figure 2.3: CcP Residue 191 Orientation. Overlay of residue 191 in the complex crystal structures shows that the side-chain holds approximately the same position in each variant. WT is shown in white, W191Y in pink, W191F in blue, and W191G in yellow. All three aromatic sidechains orient themselves in the plane of coordinating H175. In the WT, W191 forms a polar contact with D235. W191Y and W191F have no polar contacts. The backbone of W191G holds the same conformation in complex as the wild-type, despite evidence that the loop from 190 – 195 becomes very flexible as a result of the mutation.

Like the indole of W191, the phenol group of W191Y and the phenyl group of F191 are oriented to be in approximately the same plane at H175, which coordinates the heme. The nitrogen of W191 forms a hydrogen bond with D235 (Finzel, Poulos, & Kraut,

1984), but there is no polar residue in hydrogen bonding range of the Y191 hydroxyl group. In W191G, difference density confirmed the presence of ordered water molecules in the cavity created by loss of the W191 indole, consistent with structures of W191G CcP alone (Rabi A. Musah, 2002). However, the positions of the water molecules detected in our structures differ from those of the uncomplexed CcP, and vary between chain A and chain C. This is likely due to conformation changes caused by Cc binding in the crystals. Despite sufficient space available, no water molecules were detected near the sidechains Y191 or F191.

To detect ligand binding in the cavity of W191G CcP, crystals were soaked with 30 mM of various compounds, detailed in Figure 2.4. These compounds were selected based on their structural similarity to aniline or indoline, and their redox potentials, which lie near the value E^0 = 1.09 V for tryptophan in solution(DeFelippis, Murthy, Faraggi, & Klapper, 1989). Aniline and indoline have recorded affinities of 30 µM and 160 µM(Rabi A. Musah, 2002) respectively, and although the affinity of the other compounds has not been measured, it is reasonable to assume they would be in the same range, due to their structural similarity.

Figure 2.4: Hopping Site Compounds. Shown are all the compounds used for soaking crystals of the W191G CcP : Cc complex. They were chosen based on their redox potentials and their structural similarities to other compounds known to bind in the W191G cavity. Indoline, Tryptophan, and Indole may have been blocked from entering the cavity due to their larger size. Indole is also limited by its low solubility in water.

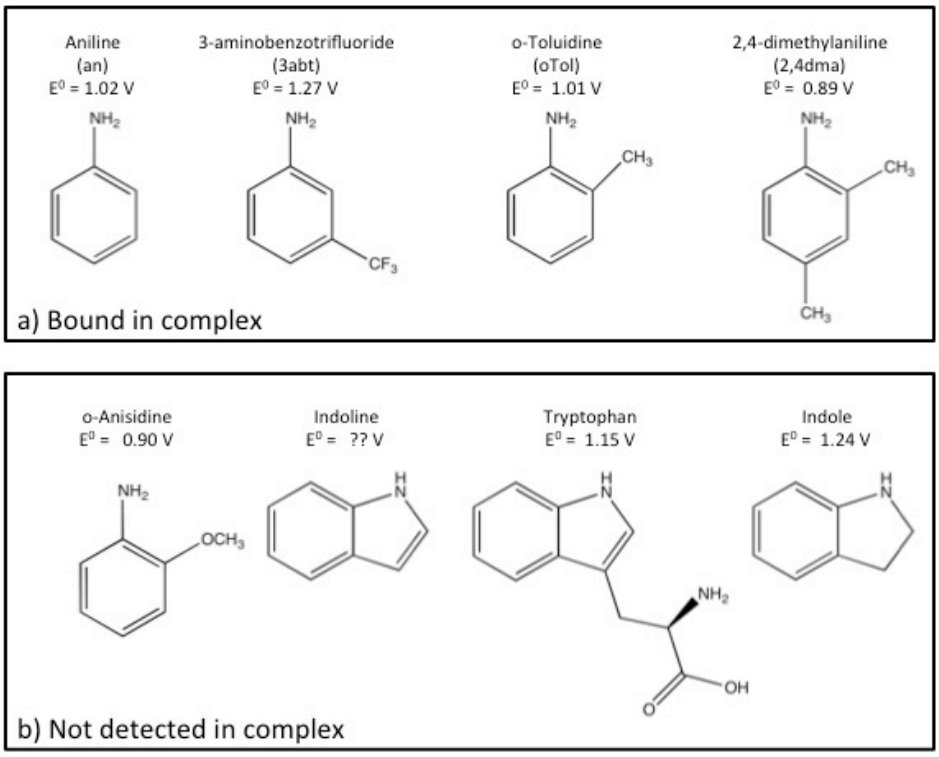

Of the many compounds tested, four were shown to bind in W191G CcP by the presence of significant difference electron density (> 2σ) in the cavity made vacant in by the W191G substitution (Figure 2.5).

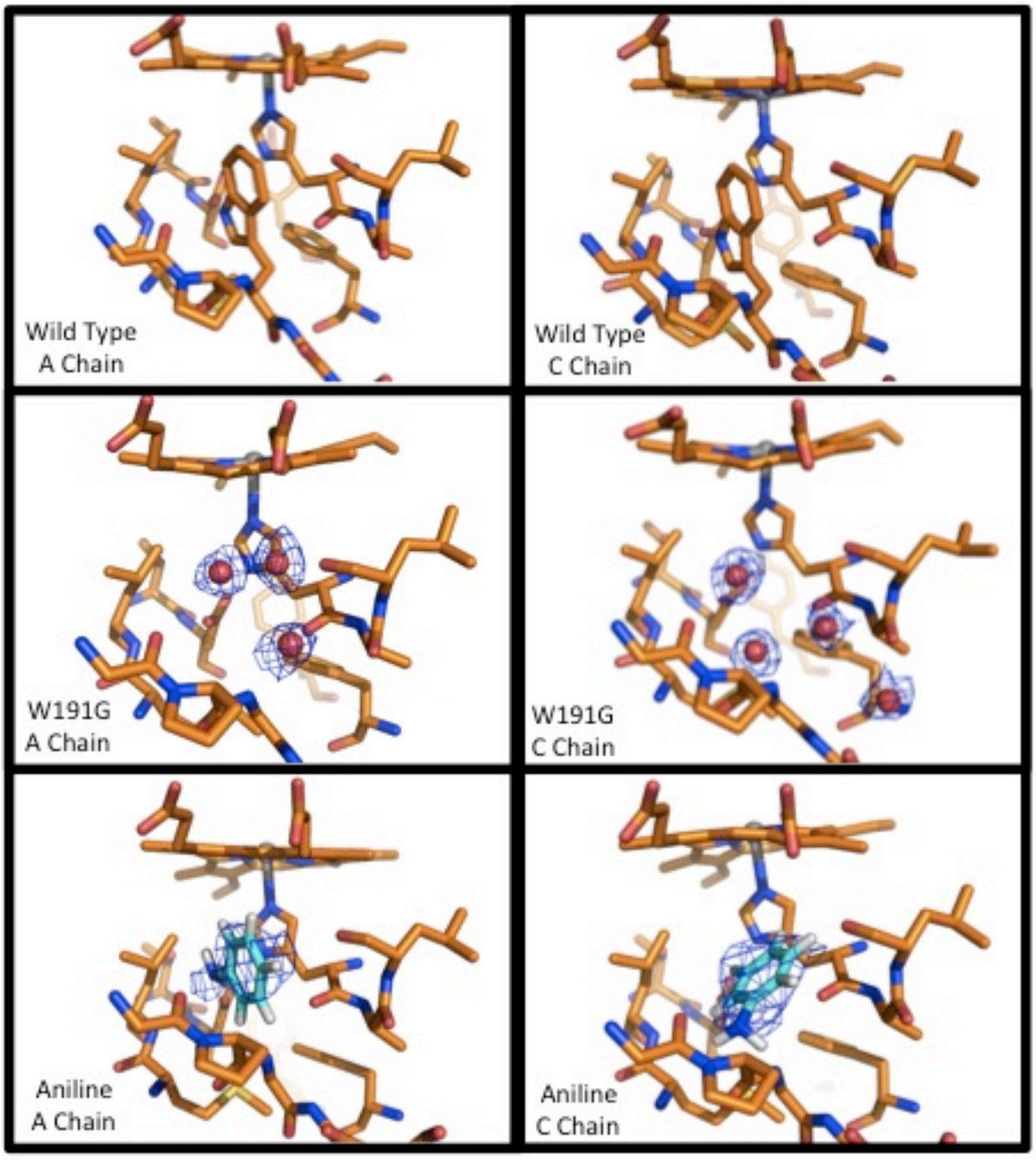

Figure 2.5: Ligands bound in the W191G CcP Cavity. Structures of W191G CcP from various crystals soaked with different compounds. The difference electron density shown is at strength sigma = 2.0 – 2.4. The structures of the ligands were fit into the density by hand and were not present during structure refinement.

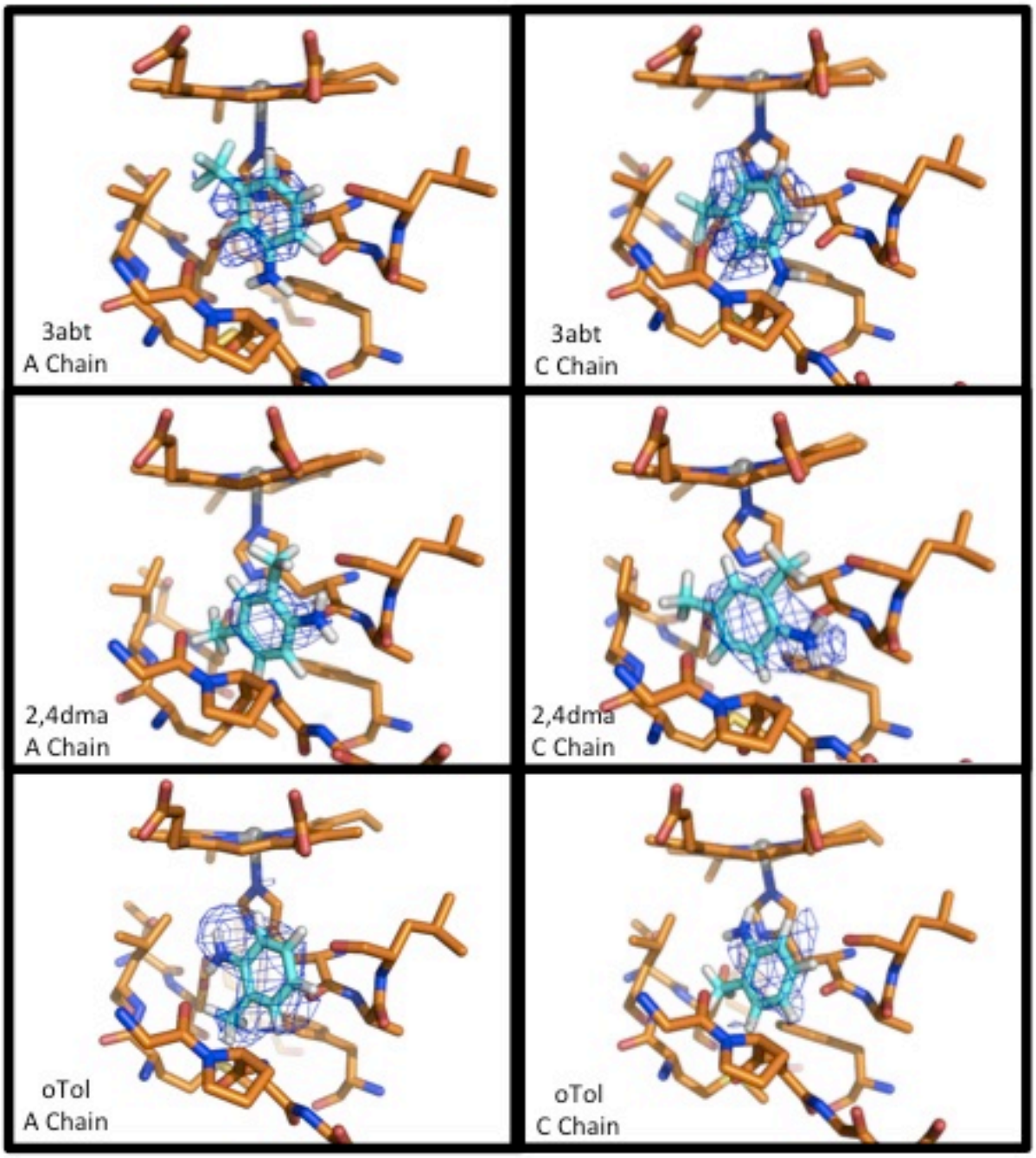

Figure 2.5 Continued

All five compounds show electron density at the same place in the cavity, which is the area that would be occupied by W191 if it were present. In most cases the electron density is ambiguously shaped, indicating that the compounds are bound in a variety of configurations. Despite its recorded affinity for the cavity, we could not detect evidence of indoline binding in the complex crystals. Perhaps its larger size prevented it from diffusing into the cavity when cytochrome c is occluding the 190 – 195 loop. The loop movement made possible by the W191G mutation may be necessary for the binding of larger compounds(Hays Putnam, Lee, & Goodin, 2009; Melissa M. Fitzgerald, 1996). The same may be true of indole and tryptophan as well. In addition, indole has extremely low solubility in aqueous solutions, which may have prevented it from reaching high enough concentrations to bind to the cavity.

Michaelis-Menten Kinetics

Both the wild-type and W191Y CcP displayed strong peroxidase activity (Figure 2.6), and the measured activity at many concentrations showed classic Michaelis-Menten behavior (Figure 2.7).

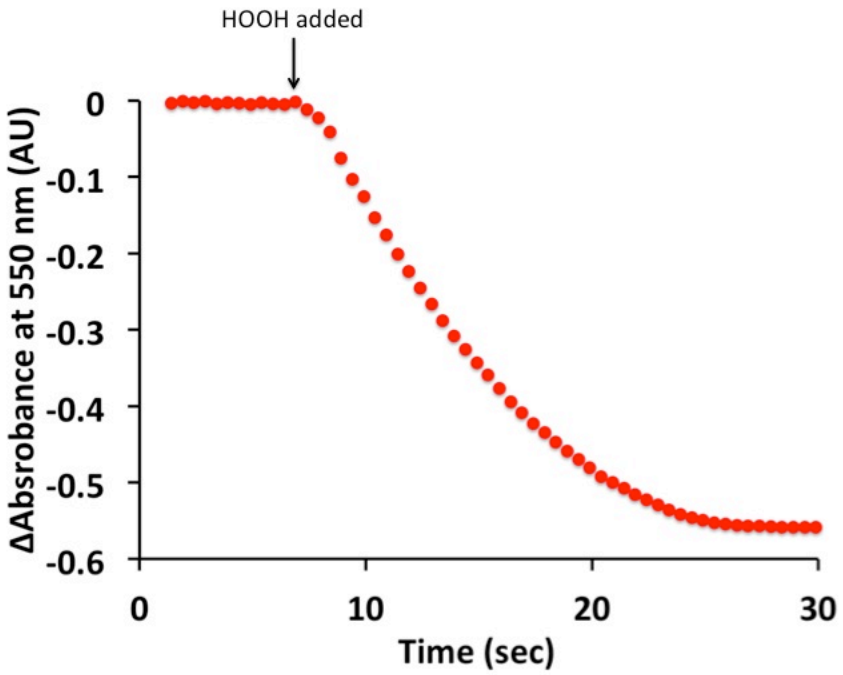

Figure 2.6: CcP Activity. Sample trace from the steady-state assay of the peroxide-driven oxidation of Cc, monitored at 550 nm. The downward curve indicates disappearance of the Fe(II) Cc peak as it reduces CcP after hydrogen peroxide is converted to water.

The measure values of V_{max} for the wild-type and W191Y are 3.00 µmoles/sec and 1.65 µmoles/sec, respectively. This agrees well with the measured value of 2.7 µmoles/sec for WT CcP with Cc (Chae Hee Kang, 1977). At these concentrations of Cc, K_m (and dissociation constant K_D) are known to vary widely with buffer strength. The values obtained for Km of 29.55 µM for the wild-type and 21.65 µM for W191Y lie within the ranges previous reported for 100 mM KPi (Volkov, Bashir, Worrall, & Ubbink, 2009).

Figure 2.7: Michaelis-Menten kinetics of CcP mutants. Michaelis-Menten curves of CcP and three mutants. Only the WT and W191Y display kinetic activity. W191G and W191F rates are equal to the rates of hydrogen peroxide oxidation of Cc.

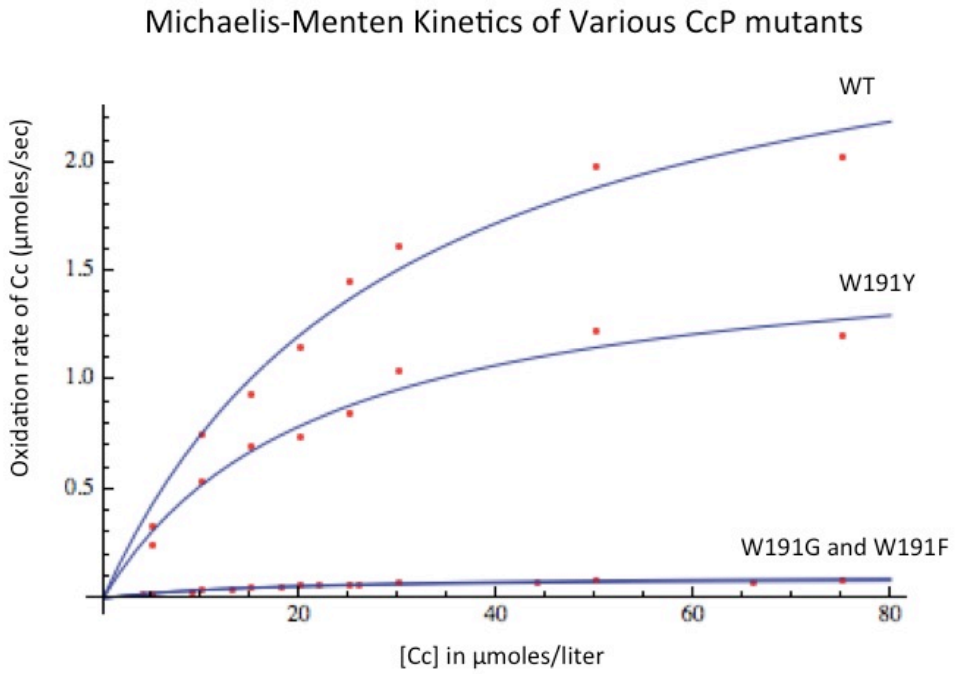

Mutants W191F and W191G had no detectable peroxidase activity. Although oxidation of Cc could be detected in the presence of hydrogen peroxide, the rates measured with the enzyme present were approximately the same as the rate of Cc oxidation by hydrogen peroxide alone. As a result, the activity of W191F and W91G was so low that any estimation of V_{max} or K_m is unreliable.

Table 2.2: Ligand Presence on Peroxidase Activity. Measured W191G and W191F CcP activity from the steady-state assay with potential hopping-site replacement ligands present. If a compound has utility as a hopping site, we should see an increase in Cc reduction when it is present with W191G but not W191F. However, no rescue of peroxidase activity was detected. For comparison, the activity of wild-type CcP at this concentration of Cc is 1,620 nmoles/sec.

Ligand	W191G Activity (nmoles/s)	W191F Activity (nmoles/s)	W191G / W191F (%)
Aniline	15.8	13.7	115
oTol	86.3	72.5	119
3abt	38.4	29.1	132
24dma	44.6	54.7	82
Anisidine	82.1	101	81
Indoline	19.5	21.3	92
Indole	12.9	13.5	96
Tryptophan	14.4	18.3	79

To determine if the small compounds shown to bind in the W191G CcP cavity can rescue peroxidase activity, the rate of Cc oxidation was measured with various ligands present in solution. Results are shown in Table 2.2. Ligand concentrations of 2 mM were used, as this is over 10 times greater than the K_D of indoline binding and 100 times greater than that of aniline(Rabi A. Musah, 2002). The K_Ds for all of the compounds are not known, but due to their structural similarity to indoline and aniline, it's like that they are similar in magnitude. As a control, we also measured the oxidation rate of Cc when ligands were present with W191F. If Cc oxidation is accelerated due to rescued

peroxidase activity, it will only be detected in the presence of W191G CcP, as W191F CcP has no cavity for the ligands to bind specifically.

Although some of the compounds, like anisidine, show a 5-fold increase in the rate of oxidation, none of the compounds showed a significantly greater effect in with W191G compared to W191F. As such, these compounds modestly accelerate the oxidation of Cc through an unknown mechanism that does not mimic the natural function of W191.

Compound 1 Detection

The formation of compound 1 is typically detected by a shift in the Soret peak of CcP from 409 nm to 420 nm and formation of alpha bands characteristic of the oxyferryl species (Yonetani, 1965). Spectra of both wild-type CcP and W191Y CcP display these features, indicating that that the W191Y mutation does not inhibit formation of the oxyferryl (Figure 2.8).

Figure 2.8: Spectra of Peroxide-bound CcP. UV/Vis spectra of CcP before (blue) and after (red) introduction of hydrogen peroxide. WT and W191Y show the typical Soret shift from 409 to 420 nm, as well as the formation of alpha bands that are indicative of Cpd I. W191F also shows a shift from 409 to 421 nm, and forms less defined alpha bands. W191G shows a shift from 414 to 417 nm, with no alpha bands detected.

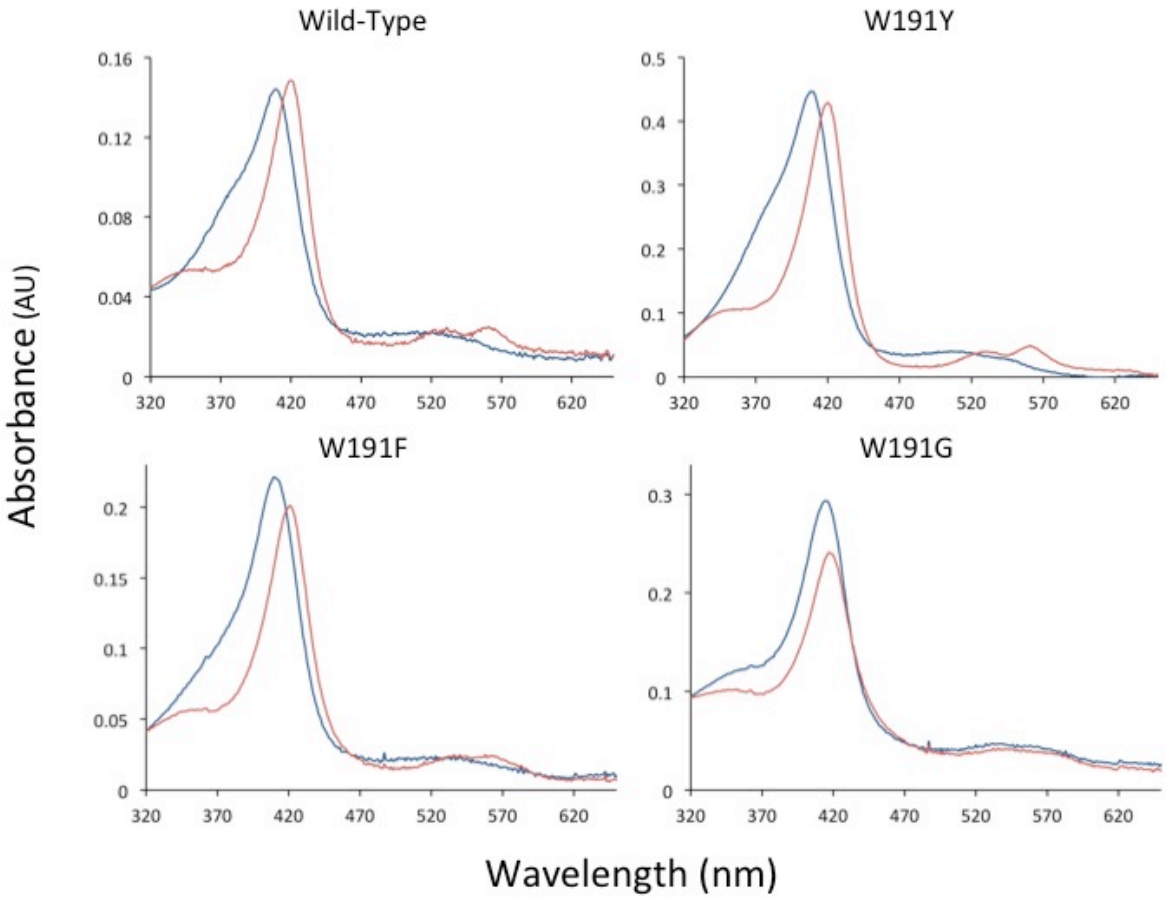

W191F also shows a similar Soret peak shift, from 409 nm to 421, but the alpha bands are less defined, which suggests that the W191F mutation perturbs the electronic environment of the heme. W191G displays the most different behavior, however. In its reduced state, W191G CcP has a Soret peak at 414 nm, unlike the rest which have their Soret peak at 409 nm, and upon mixing with hydrogen peroxide, shifts to 417 nm with no significant change in the alpha bands. While the peroxide is having an effect on the

electronic state of W191G CcP, it's unclear what the interaction is, and if it could be termed Cpd1.

The other hallmark of Cpd1 is the formation of an organic radical at W191. To directly detect the radical, continuous wave EPR spectra were measured of the CcP WT and variants after reaction with hydrogen peroxide (Figure 2.9). Note that CcP Cmpd I is relatively stable and will persist in aerobic solution for > 10 min once formed. The shape and location of the EPR signal for wild-type CcP is consistent with that of a W191 radical(Ivancich, Dorlet, Goodin, & Un, 2001). The observation of peak splitting upon solvent exchange into D_2O supports the previous conclusion that the tryptophan radical is a protonated cation. However, previous measurements of compound 1 detected these features in the presence of H_20, despite similar parameters for the spectroscopy. One possible explanation is that the previous measurements were carried out at concentration 2 - 3 times greater than ours, allowing for a stronger signal. Another explanation is that the strong hydrogen bonds formed in D_2O perturb the conformation of the protein, perhaps changing the hydrogen bond length between D235 and W191.

Figure 2.9: EPR spectra of CcP Compound 1. H2O spectra are shown in blue, D2O spectra in red. The emergence of new features in the WT after deuterium exchange may reflect that the Cpd1 radical is protonated, or possibly a change in the homogeneity of the sample. Similar effects are not seen for the W191Y radical, which is likely to be unprotonated. Both WT and W191Y radical signals are much larger than that seen in W191G or W191F (not shown). It is likely that small amount of Tyr radical is formed elsewhere in the protein in W191G.

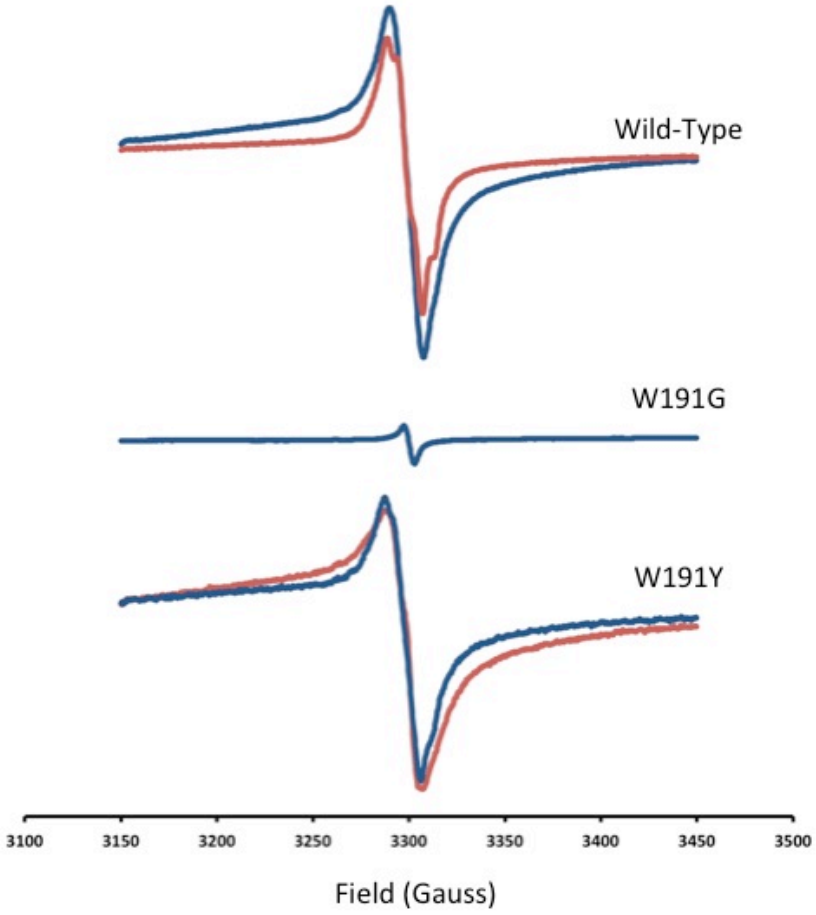

W191Y with hydrogen peroxide displayed a signal equal in magnitude to the wild-type, with a shape characteristic of a tyrosine radical(Debus, Barry, Babcock, & McIntosh, 1988). The signal lacked distinguishing features, indicating that the tyrosine lacks polar contacts, and the spectral shape did not change upon deuteration, suggesting that the hydroxyl group of the radical is deprotonated.

W191G with hydrogen peroxide displayed a signal with about 1/10 the magnitude of the wild-type, which agrees with previously measured spectra(Ivancich et al., 2001). It has been suggested that one of several other tyrosines in the protein may form a radical in the absence of W191, but because of their distance from the heme, the efficiency of electron transfer is low and thus only a small radical population is generated at these remote sites.

4. Discussion

For a hopping site to be effective, it is predicted that its potential must be greater than the donor molecule and not more than 200 mV greater than the acceptor molecule (Shih et al., 2008). In CcP, it has been measured that reduction potential of Fe(IV=O) CcP to Fe(III) CcP is $E^0 = 1.09$ V (Purcell & Erman, 1976), and that the potential of $W191^+$ in solution ranges from 0.9 to 1.09 V in solution (DeFelippis et al., 1989). The potential would likely be slightly changed in the protein environment. As the potential of Fe(II) Cc is 0.290 V(Purcell & Erman, 1976), W191 meets both of these conditions by being able to be oxidized by the Fe(IV=O) heme, and then being able to oxidize Fe(II) Cc.

Together with the rapid back ET observed in the W191Y ZnCcP system in Chapter 1, the high peroxidase activity observed here suggests that Y191 is as active a hopping site as W191. EPR and UV/Vis spectroscopy proves that $Y191^{\bullet}$ forms upon hydrogen peroxide binding. Although we do not know the potential of the $Y191^{\bullet}$ CcP state,

measurements of $Trp^{\bullet}$ solution place E^0 in the range 0.96 – 1.09 V, and $Y^{\bullet}$ in the range 0.92 – 0.97(DeFelippis et al., 1989). These measurements do not take into account protonation state, but this small difference in potential would keep it well between the potentials of Fe(IV=O) CcP and Fe(II) Cc. The crystal structure shows that Y191 is exactly the same distance from the heme of Cc as W191 is, and it does not perturb the geometry of the porphyrin metal, so the only change will be in the driving force, which in turn will be a function of protonation state.

The Trp radical is clearly protonated in Cmpd I, but this is not necessarily the case for the Tyr radical. Tyrosine is observed to always undergo proton-coupled ET (PCET) when oxidized (Hoganson & Tommos, 2004; Warren, Winkler, & Gray, 2012), and the structure shows no polar contacts for the hydroxyl group to interact with. However, even though no structured water is observed near Y191, there is sufficient space, and it is likely that transient water molecules share polar contact with Y191. An interesting experiment in the future would be to measure the peroxidase or ET activity as a function of pH.

Phenylalanine has a greater oxidation potential than tyrosine and tryptophan, and the inability of F191 to form a radical or engage in peroxidase activity suggests that its potential lies more than 0.2 V above that of Fe(IV=O) CcP. The slow back ET kinetics in Chapter 1 support this.

Having no sidechain to oxidize, W191G also displays little peroxidase activity. Previous studies in trying to complement the cavity in W191G with an indole-bearing peptide also showed failure to rescue peroxidase activity(Hays Putnam et al., 2009), even though the indole was shown to bind strongly in the cavity and even hydrogen bond with D235. Since a range of compounds of redox potential similar to that of tryptophan in solution was known to bind in the compound, we investigated the possibility that they could act as a surrogate hopping site. Although structural studies show us that some of the compounds can bind in the cavity and even localize where the W191 indole would be, peroxidase activity was not rescued. The ambiguous shape of the electron density suggests that these compounds may be quite mobile within the pocket.

Artificial hopping sites have been shown to be effective in synthetic peptides(Giese et al., 2005), where they were bound to the same peptide backbone as the acceptor molecule. Although most evidence points to superexchange being the dominant mechanism of interprotein ET, it may be that a covalent bond to the donor molecule assists in creating an active hopping site by fixing the position of the redox active moiety.

5. Bibliography

Adams, Paul D, Afonine, Pavel V, Bunkoczi, Gábor, Chen, Vincent B, Davis, Ian W, Echols, Nathaniel, . . . Grosse-Kunstleve, Ralf W. (2010). PHENIX: a comprehensive Python-based system for macromolecular structure solution. *Acta Crystallographica Section D: Biological Crystallography, 66*(2), 213-221.

Brunger, Axel T, Adams, Paul D, Clore, G Marius, DeLano, Warren L, Gros, Piet, Grosse-Kunstleve, Ralf W, . . . Pannu, Navraj S. (1998). Crystallography & NMR system: A

new software suite for macromolecular structure determination. *Acta Crystallographica Section D: Biological Crystallography, 54*(5), 905-921.
Burda, Květoslava. (2007). Dynamics of electron transfer in photosystem II. *Cell biochemistry and biophysics, 47*(2), 271-284.
Chae Hee Kang, Shelagn Ferguson-Miller, and E. Margoliash. (1977). Steady State Kinetics and Binding of Euakryotic Cytochromes c with Yeast Cytochrome c Peroxidase. *J Biol Chem, 252*(3), 919-926.
Cordes, M., & Giese, B. (2009). Electron transfer in peptides and proteins. *Chem Soc Rev, 38*(4), 892-901. doi: 10.1039/b805743p
Cordes, M., Kottgen, A., Jasper, C., Jacques, O., Boudebous, H., & Giese, B. (2008). Influence of amino acid side chains on long-distance electron transfer in peptides: electron hopping via "stepping stones". *Angew Chem Int Ed Engl, 47*(18), 3461-3463. doi: 10.1002/anie.200705588
Debus, Richard J, Barry, Bridgette A, Babcock, Gerald T, & McIntosh, Lee. (1988). Site-directed mutagenesis identifies a tyrosine radical involved in the photosynthetic oxygen-evolving system. *Proceedings of the National Academy of Sciences, 85*(2), 427-430.
DeFelippis, Michael R., Murthy, C. P., Faraggi, M., & Klapper, Michael H. (1989). Pulse radiolytic measurement of redox potentials: the tyrosine and tryptophan radicals. *Biochemistry, 28*(11), 4847-4853. doi: 10.1021/bi00437a049
Emsley, Paul, & Cowtan, Kevin. (2004). Coot: model-building tools for molecular graphics. *Acta Crystallographica Section D: Biological Crystallography, 60*(12), 2126-2132.
English, Brian P, Min, Wei, van Oijen, Antoine M, Lee, Kang Taek, Luo, Guobin, Sun, Hongye, . . . Xie, X Sunney. (2005). Ever-fluctuating single enzyme molecules: Michaelis-Menten equation revisited. *Nat Chem Biol, 2*(2), 87-94.
Finzel, Barry Craig, Poulos, Th L, & Kraut, J. (1984). Crystal structure of yeast cytochrome c peroxidase refined at 1.7-A resolution. *Journal of Biological Chemistry, 259*(21), 13027-13036.
Fitzgerald, Melissa M, Churchill, Michael J, McRee, Duncan E, & Goodin, David B. (1994). Small molecule binding to an artificially created cavity at the active site of cytochrome c peroxidase. *Biochemistry, 33*(13), 3807-3818.
Giese, B., Napp, M., Jacques, O., Boudebous, H., Taylor, A. M., & Wirz, J. (2005). Multistep electron transfer in oligopeptides: direct observation of radical cation intermediates. *Angew Chem Int Ed Engl, 44*(26), 4073-4075. doi: 10.1002/anie.200500391
Gray, Harry B, & Winkler, Jay R. (2003). Electron tunneling through proteins. *Quarterly reviews of biophysics, 36*(3), 341-372.
Hays Putnam, A. M., Lee, Y. T., & Goodin, D. B. (2009). Replacement of an electron transfer pathway in cytochrome c peroxidase with a surrogate peptide. *Biochemistry, 48*(1), 1-3. doi: 10.1021/bi8020263
Hoganson, Curtis W, & Tommos, Cecilia. (2004). The function and characteristics of tyrosyl radical cofactors. *Biochimica et Biophysica Acta (BBA)-Bioenergetics, 1655*, 116-122.
Ivancich, Anabella, Dorlet, Pierre, Goodin, David B, & Un, Sun. (2001). Multifrequency high-field EPR study of the tryptophanyl and tyrosyl radical intermediates in wild-type and the W191G mutant of cytochrome c peroxidase. *J Am Chem Soc, 123*(21), 5050-5058.

Jasion, V. S., Doukov, T., Pineda, S. H., Li, H., & Poulos, T. L. (2012). Crystal structure of the Leishmania major peroxidase-cytochrome c complex. *Proc Natl Acad Sci U S A, 109*(45), 18390-18394. doi: 10.1073/pnas.1213295109

Lukacs, A., Eker, A. P., Byrdin, M., Brettel, K., & Vos, M. H. (2008). Electron hopping through the 15 A triple tryptophan molecular wire in DNA photolyase occurs within 30 ps. *J Am Chem Soc, 130*(44), 14394-14395. doi: 10.1021/ja805261m

Melissa M. Fitzgerald, Rabi A. Musah, Duncan E. McRee, and David B. Goodin. (1996). A ligand-gated, hinged loop rearrangement opens a channel to a buried artificial protein cavity. *Nature Structural Biology, 3*(7), 626 - 630.

Otwinowski, Z, & Minor, W. (1997). Processing of X-ray diffraction data. *Methods in enzymology, 276*, 307-326.

Page, Christopher C, Moser, Christopher C, Chen, Xiaoxi, & Dutton, P Leslie. (1999). Natural engineering principles of electron tunnelling in biological oxidation–reduction. *Nature, 402*(6757), 47-52.

Purcell, WL, & Erman, James E. (1976). Cytochrome c peroxidase catalyzed oxidations of substitution inert iron (II) complexes. *J Am Chem Soc, 98*(22), 7033-7037.

Rabi A. Musah, Gerard M. Jensen, Steven W. Bunte, Robin J. Rosenfeld, and David B. Goodin. (2002). Artificial Protein Cavities as Specific Ligand-binding Templates: Characterization of an Engineered Heterocyclic Cation-binding Site that Preserves the Evolved Specificity of the Parent Protein. *J Mol Biol, 315*, 845 - 857.

Rich, PR. (2003). The molecular machinery of Keilin's respiratory chain. *Biochemical Society Transactions, 31*(6), 1095-1106.

Seifert, J. L., Pfister, T. D., Nocek, J. M., Lu, Y., & Hoffman, B. M. (2005). Hopping in the electron-transfer photocycle of the 1:1 complex of Zn-cytochrome c peroxidase with cytochrome c. *J Am Chem Soc, 127*(16), 5750-5751. doi: 10.1021/ja042459p

Seyedsayamdost, M. R., Xie, J., Chan, C. T., Schultz, P. G., & Stubbe, J. (2007). Site-specific insertion of 3-aminotyrosine into subunit alpha2 of E. coli ribonucleotide reductase: direct evidence for involvement of Y730 and Y731 in radical propagation. *J Am Chem Soc, 129*(48), 15060-15071. doi: 10.1021/ja076043y

Shih, C., Museth, A. K., Abrahamsson, M., Blanco-Rodriguez, A. M., Di Bilio, A. J., Sudhamsu, J., . . . Gray, H. B. (2008). Tryptophan-accelerated electron flow through proteins. *Science, 320*(5884), 1760-1762. doi: 10.1126/science.1158241

Volkov, A. N., Bashir, Q., Worrall, J. A., & Ubbink, M. (2009). Binding hot spot in the weak protein complex of physiological redox partners yeast cytochrome C and cytochrome C peroxidase. *J Mol Biol, 385*(3), 1003-1013. doi: 10.1016/j.jmb.2008.10.091

Warren, Jeffrey J, Winkler, Jay R, & Gray, Harry B. (2012). Redox properties of tyrosine and related molecules. *FEBS letters, 586*(5), 596-602.

Yonetani, Takashi. (1965). Studies on Cytochrome c Peroxidase II. Stoichiometry Between Enzyme, H2O2, and ferrocytochrome c and enzymic determination of extinction coefficients of cytochrome c. *Journal of Biological Chemistry, 240*(11).

6.